geologica acta

Citation: Larena, Z., Arenas, C., Ortiz, J.E., Sanjuan, J., Pascual, A., Larraz, M., Murelaga, X., Baceta, J.I., 2025. Quaternary tufas of the Inglares River valley: An example of changing slope stepped fluvial system, Álava, N Spain. Geologica Acta, 23.10, 1-32, I-III.
Online ISSN: 1696-5728 DOI: 10.1344/GeologicaActa2025.23.10

Quaternary tufas of the Inglares River valley: An example of changing slope stepped fluvial system, Álava, N Spain

Zuriñe Larena[1] Concha Arenas[2*] José Eugenio Ortiz[3] Josep Sanjuan[4] Ana Pascual[1] Mariano Larraz[5] Xabier Murelaga[1] Juan Ignacio Baceta[1]

[1]Departamento de Geología, Facultad de Ciencia y Tecnología. Euskal Herriko Unibertsitatea UPV/EHU
Apartado 644, E-48080 Bilbao. Larena Email: zurine.larena@ehu.eus, ORCID: 0000-0003-0958-2599; Murelaga Email: xabier.murelaga@ehu.eus, ORCID: 0000-0001-8049-4917; Baceta Email: juanignacio.baceta@ehu.eus, ORCID: 0000-0003-3154-225.

[2]Department of Earth Sciences, Institute for Research on Environmental Sciences of Aragón (IUCA) and GeoTransfer Group, University of Zaragoza
12 Pedro Cerbuna St, 50009 Zaragoza, Spain. Email: carenas@unizar.es, ORCID: 0000-0002-4212-0524.

[3]Laboratory of Biomolecular Stratigraphy. E.T.S.I Minas y Energía, Universidad Politécnica de Madrid
21 Ríos Rosas St, 28003 Madrid, Spain. Email: joseeugenio.ortiz@upm.es, ORCID: 0000-0002-5699-2593.

[4]Departamento de Dinámica de la Tierra y del Océano, Facultad de Ciencias de la Tierra
Martí i Franqués, s/n, E-08028 Barcelona. Email: josepsanjuan@ub.edu, ORCID: 0000-0002-1275-6783.

[5]Departamento de Biología Ambiental (Zoología). Facultad de Ciencias, Universidad de Navarra
Apartado 177, E-31080 Pamplona. Email: mlarraz@external.unav.es, ORCID: 0000-0001-8891-5018.

*Corresponding autor

ABSTRACT

This study examines the factors that controlled the formation of Quaternary calcareous tufa deposits along the valley of the Inglares River (Álava, north Spain), currently fed by a karst-carbonate aquifer. It is based on stratigraphic, chronological (Amino Acid Racemisation, AAR), sedimentological, and $\delta^{13}C$ and $\delta^{18}O$ analyses, complemented by palaeontology (molluscs, ostracods and charophytes). The examined deposits occur as isolated bodies in the uppermost and downmost stretches of the valley, reaching 45 and 25m in thickness, respectively. AAR dating classified them into two groups: Middle–Late Pleistocene (MIS 5e) and Middle and Late Holocene (MIS 1). The former only occurred in the downstream stretch. Up to eleven carbonate facies and minor allochthonous coarse detrital facies have been characterised and arranged into four distinct facies associations. Their features and bedding geometries suggested two main depositional settings: a low- to moderate-slope stepped stretch with small barrage cascades, dammed areas, and abundant palustrine zones (downstream system) and a high-slope stretch with steep stepped cascades and pools (upstream system). These settings respond to bedrock lithology and structural changes throughout the valley, which appear to be the principal factors controlling the tufa depositional architecture. Based on $\delta^{13}C$, an increase in aridity was inferred from the Middle–Late Pleistocene to Holocene. The isotopic differences between the upstream and downstream Holocene tufa might reflect the spatial evolution of $\delta^{13}C$ and $\delta^{18}O$ in stream water through the approximately 8km long surveyed transect. Erosion due to sudden changes in water discharge may have caused the stratigraphic gap between the two tufa groups.

KEYWORDS **Fluvial tufa. Sedimentology. Facies model. Quaternary climate. North Iberia.**

INTRODUCTION

Sedimentary tufas are calcium carbonate deposits formed from meteoric water at ambient temperature, mainly on biotic substrates (*e.g.* macrophytes, bryophytes, algae, microbes) and also embody a variety of allied carbonate deposits (*e.g.* mollusc and ostracod limestones). They have been the focus of numerous studies that address various issues, including geomorphology, hydrochemistry, palaeobotany, and sedimentology (Heiman and Sass, 1989; Ordóñez and García del Cura, 1983; Pedley *et al.*, 1990; Pentecost, 2005). In recent decades, many studies have relied on the palaeoclimatic implications of tufas because their formation seems to be favoured by warm and wet climatic conditions (Andrews *et al.*, 1997; Capezzuoli *et al.*, 2010; Durán, 1989; Henning *et al.*, 1983; Martín Algarra *et al.*, 2003). Most Quaternary tufa deposits coincide with warm odd Marine Isotope Stages (MIS) (*e.g.* Gibbard *et al.*, 2005), particularly MIS 7, MIS 5, and MIS 1 (*e.g.* Durán, 1989; Martín Algarra *et al.*, 2003), but those from cool MIS 8 and MIS 6 have also been documented (Capezzuoli *et al.*, 2014; Sancho *et al.*, 2015). Ancient tufa deposits have formed under varied climatic conditions, ranging from temperate-wet to semi-arid (Cremaschi *et al.*, 2010; Moeyersons *et al.*, 2006; Viles *et al.*, 2007). Moreover, these carbonates are currently being formed over a wide range of climatic conditions, provided that the water is saturated with respect to calcium carbonate (Arenas-Abad *et al.*, 2010; Vázquez-Urbez *et al.*, 2012). They are common features in freshwater carbonate rivers and lakes but can also occur in saline and alkaline lakes (Della Porta, 2015; Pentecost, 2005).

Therefore, in addition to climate, other factors have a direct influence on tufa formation, including the topography of the basin (mostly dependent on bedrock lithology and tectonic structure) and the characteristics of the associated aquifer (dependent on local and regional geological features) (Arenas-Abad *et al.*, 2010; Viles and Pentecost, 2007). Studies integrating both extrinsic (climate, hydrology, and topography) and intrinsic factors (*e.g.* flora development and hydrochemistry) should lead to more adjusted results and a better understanding of tufa development at medium-long temporal scales. At much shorter decadal to seasonal scales, temperature and precipitation can exert direct control on some depositional (*e.g.* thickness, texture, and sedimentary structures) and geochemical features (Arenas *et al.*, 2014a), including the formation of laminated and banded microbial deposits (Arenas and Jones, 2017; Brasier *et al.*, 2010; Matsuoka *et al.*, 2001).

Palaeobotanical (Aranbarri *et al.*, 2016; Rubio-Millán, 2002) and $\delta^{13}C$ and $\delta^{18}O$ data (Kano *et al.*, 2007; Osácar *et al.*, 2013) of these carbonate facies have been used as proxies for the characterisation of depositional, hydrological and climatic inferences on different scales, from seasonal to 100-Ky spans. For long periods, $\delta^{13}C$ values can help to identify fluctuations in humidity and variations in the proportion of C4/C3 plants (Andrews *et al.*, 2000; Doran *et al.*, 2015). However, in some cases, these deductions are not possible as they are somehow conditioned by the age of the tufas studied. The commonly associated freshwater biota, including gastropods and ostracods, may also provide important clues regarding water composition, average temperature, and nutrient levels (Dillon, 2000; Ruiz *et al.*, 2013).

This work provides the results of a multiproxy study of the outcropping Quaternary fluvial tufa deposits that formed along the valley of the Inglares River, Álava province (Spain), based on stratigraphical, chronological and sedimentological analyses, coupled with $\delta^{13}C$ and $\delta^{18}O$ data and complemented with preliminary palaeontological (molluscs, ostracods and charophytes) information of the carbonate facies. This study, i) examined the depositional stages of these tufas, ii) proposed a sedimentary facies model for their development and iii) discussed the factors that favour their formation and control the evolution of the fluvial network over time. The results are relevant for interpreting the hydrological and climatic significance of the sedimentary depositional and geochemical features in other fluvial carbonate systems in the geological record, and highlight the potential of present and ancient tufa accumulations as educational and tourism resources in this region and elsewhere.

GEOGRAPHICAL AND GEOLOGICAL CONTEXT

The study area is located North of the Iberian Peninsula, 23km Southwest of Vitoria-Gasteiz, and 8km North of Haro (Fig. 1). The examined Quaternary tufas crop out along the present Inglares River valley, a tributary of the Ebro River that runs East-West along a South vergent fold and thrust belt made of Cretaceous–lower Palaeogene sedimentary units. This tectonic system represents the western prolongation of the South Pyrenenan Thrust Front system (SPTF) over the Ebro foreland basin (Figs. 1; 2A). Along the Inglares Valley, a great variety of Mesozoic to Palaeogene carbonate and siliciclastic units occur. In the upper and middle river courses, the substrate is mostly defined by Upper Cretaceous marine limestones and dolostones, Lower Cretaceous siliciclastics, and Jurassic carbonates. Downstream, close to the Ebro River, the Inglares River runs over uppermost Cretaceous clastic rocks, Palaeocene marine carbonates, and upper Eocene to Oligocene continental carbonate and siliciclastic deposits (Fig. 2A). It should be noted that in two specific areas, the river flows over the Upper Triassic mudstones and evaporites (Keuper facies), which define the core of two-

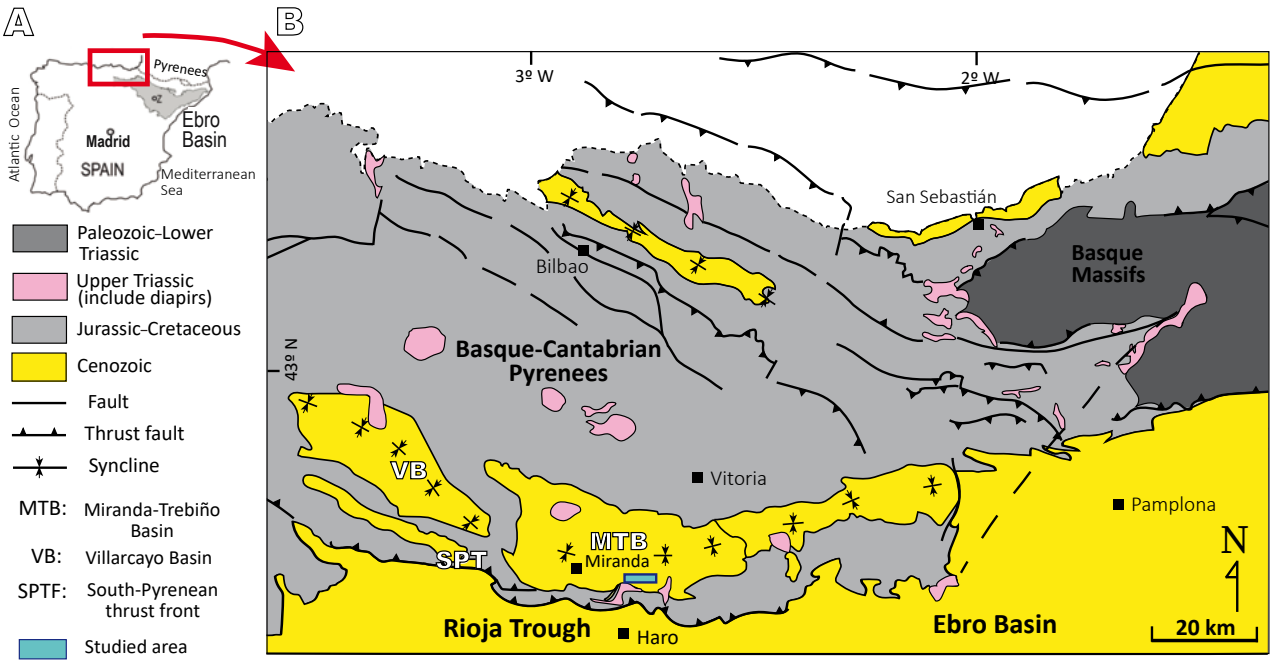

FIGURE 1. Geographical and geological location of the study area. A) Location of the study area in the Iberian Peninsula, North of Spain. B) General geological map of the Miranda-Trebiño Basin. Blue box corresponds to the study area.

kilometre-wide diapiric structures (the Peñacerrada and the Herrera-Buradón diapirs) (Fig. 2A).

The studied tufas are distributed over a few places along the valley, particularly near the Herrerías waterfall and at the Tobal outcrop on the western flanks of the aforementioned diapirs (Figs. 2A; 3). In the regional geological maps, these tufa deposits were defined as "Holocene travertines" (Portero *et al.*, 1979). In some areas upstream and downstream of the two main tufa accumulations, fine-grained, loose tufa deposits are exposed on riverbanks and adjacent floodplains, some of which occupy large areas used for agricultural activities. These were mapped as "Holocene detrital and travertine alluvial deposits" (Portero *et al.*, 1979) (Fig. 3).

The Inglares River is a 42.65km long course draining an area *ca* 91.32km^2. It begins near the San León peak (1,085m a.s.l., Sierra de Cantabria) and enters the Ebro River close to the locality of Miranda de Ebro (Fig. 1). The maximum elevation difference between the head and mouth was 640m, with an average slope of *ca* 2%. However, the river slope changes significantly along its course (Fig. 3). Taking advantage of the 163m difference in elevation between Peñacerrada and Berganzo is the electrical production of *Eléctrica-hidráulica Alavesa S.A.*, with a hydroelectric power plant *ca* 500m downstream of Berganzo (Fig. 3) (Vera and López, 1921). Only one important tributary, La Mina Creek, is located on the left bank of the Inglares River (Fig. 2A).

The Inglares River is sourced from the Sierra de Cantabria aquifer system (Key ES091MSBT022; *Confederación Hidrográfica del Ebro*; www.chebro.es), which is mostly found in Upper Cretaceous carbonate rocks with complex tectonic structures. This karstic aquifer has an irregular discharge regime (*Confederación hidrográfica del Ebro*, https://portal.chebro.es/web/guest/masas-de-agua-subterranea; https://portal.chebro.es/red-piezometrica-oficial). Mean water discharge of the Inglares River since August 2001 to February 2024 was 0.405m^3/s, measured at an upstream gauging station approximately 1km downstream of Peñacerrada. The highest values were observed in winter and spring (Discharge data from *Instituto Geográfico Nacional* and *URA, Agencia Vasca del Agua*; https://www.uragentzia.euskadi.eus/datos-de-estaciones-de-aforo/webura00-contents/es/). Several springs have been reported through the valley, at Peñacerrada (ca 715m a.s.l.; discharge= 0.05m^3/s), to the East of Berganzo (601m a.s.l) and at Ocio locality (ca 522m a.s.l.); two waterfalls have also been reported, with largest one being the Herrerías waterfall (662m a.s.l) (Fig. 3), and a *ca* 40m-high steep, stepped fall (Figs. 2A; 3). Water at the Peñacerrada spring is of calcium bicarbonate type (mean values of Ca= 92.0mg/L; HCO_3^-= 323.4mg/L), with mean pH= 7.4 and mean conductivity= 504μS/cm. (Water from 2022 and 2023, from *URA, Agencia Vasca del Agua;* https://www.uragentzia.euskadi.eus/inicio/).

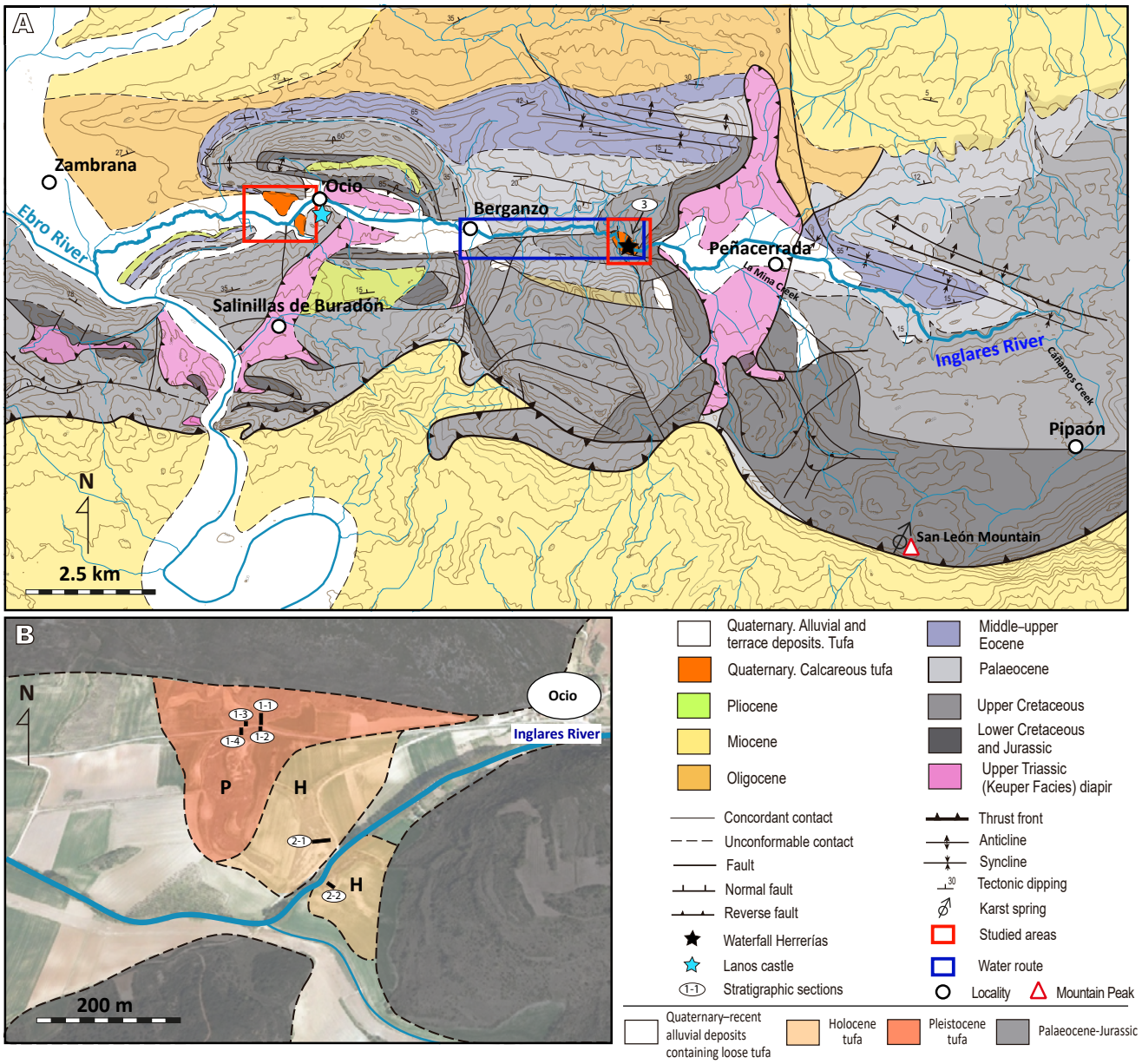

FIGURE 2. A) Geological map of the Inglares River valley. Adapted from 1:50.000 geological sheets n. 169, Casalarreina (Portero *et al.*, 1978), and 170, Haro (Portero *et al.*, 1979), of the *Instituto Geológico y Minero de España* (IGME). Location of measured stratigraphic section 3 (Herrerías) is indicated over the right red box. B) Detailed geological map of the western red box in Figure 2A. Distribution of the Pleistocene and Holocene tufa deposits and location of measured stratigraphic sections (Ocio-1: 1-1 to 1-4; Ocio-2: 2-1 and 2-2).

The present climate in the region is continental, with an average annual temperature of 18ºC, reaching maximum average values of 29ºC in July and August, and minimum average values of 9ºC in the coldest winter months. Precipitation values in this region are quite regular, with relatively higher peaks during spring (80mm on average from March to May and 85mm in June), winter (62mm in December to 97mm in January) and autumn (34mm in September to 80mm in November), and with the rainiest month being February (100mm). Summer is the driest period (minimum precipitation of 30mm in August). The average annual rainfall was 795mm (https://climaytiempo.es/espana/berganzo-3542317/).

At present, calcite tufa is actively formed through several stretches of the Inglares River (*e.g.* segment B in Fig. 3) in short cascades, rapids, and small pools. This feature represents a landscape resource for people visiting the region, known as the *Berganzo water route*, or the *Inglares water route,* hereafter referred as the *Water*

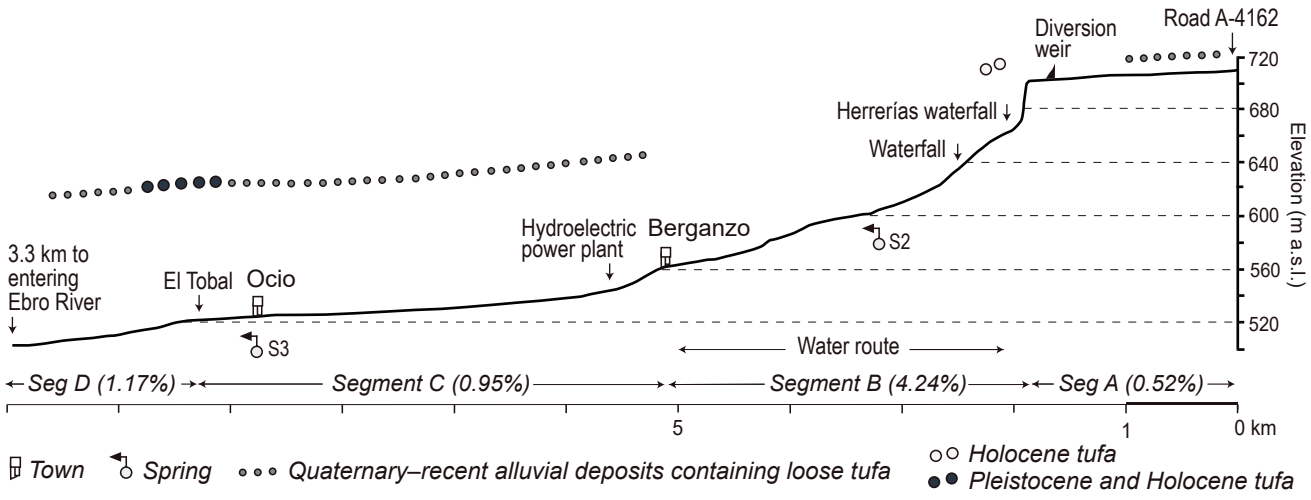

FIGURE 3. Longitudinal profile of the Inglares River (E-W section) and tufa distribution, from road A-4162 to 3.3km upstream from the Ebro River). Segments are differentiated according to changes in slope.

route (Fig. 3), (https://rutadelaguaberganzo.eu/; https://es.wikiloc.com/rutas-senderismo/ruta-del-agua-inglares-berganzo-6821270).

It is important to note that the Ocio tufa deposits are catalogued as a site of geological interest (Spanish labelled as *LIG 74: Travertinos de Ocio*) by the Basque Country Government (https://www.euskadi.eus/informacion/lugares-de-interes-geologico/web01-a2ingdib/es/). Moreover, in the past, some tufa deposits were mined locally for different purposes, including the building of houses in the Ocio and Berganzo villages and the construction of the walls of the Llanos castle. All these attributes, along with the geological information reported in this paper, reinforce the potential of the area for educational and touristic use, thus strongly supporting the need for its preservation.

MATERIALS AND METHODS

Geological information from the 1:50,000 geological sheets n. 169 (Casalarreina) and 170 (Haro) (Portero *et al.*, 1978, 1979) was superimposed on a 1:10,000 topographic basis, where new information gathered through this research on the Quaternary outcrops was added (Fig. 2). Seven stratigraphic sections were measured on a 1:100 scale: Ocio-1-1, Ocio-1-2, Ocio-1-3, Ocio-1-4, Ocio-2-1, Ocio-2-2, and Herrerías (Figs. 4; 5; 6; location of the sections in Fig. 2A, B). Sedimentological drawings were created based on field observations and photographs. The correlation between several studied sections and deposits was based on the lateral continuity of outcrops (*i.e.* tracing of key surfaces) and the age data provided by amino acid racemisation.

A set of forty-one compact and loose rock samples were collected in the field for diverse types of analyses. Thirty-two thin sections were prepared for textural and sedimentological characterisation using petrographic microscopy. The thin sections were prepared at the *Servicio General de Preparación de rocas y materiales duros* of the *Servicio General de Apoyo a la Investigación (SAI)* of the University of Zaragoza (Spain). Petrographic observations were made using an Olympus AX70-TF microscope of the *Servicio de Microscopía* Óptica *e Imagen* of the *SAI*. Scanning Electron Microscopy (SEM) observations of nine samples (freshly broken fragments, then coated with carbon) complemented the petrographic characterisation. SEM facility was a Carl Zeiss MERLIN™ FESEM; Zeiss AG, operating at 3 to 15kV and 158pA, which belonged to the *Servicio de Microscopía electrónica de materiales* of the SAI.

The mineralogical compositions of nineteen samples were obtained by X-Ray Diffraction (XRD) of the powder samples. Analyses were performed at the X-Ray Diffraction Services Unit of Rocks and Minerals of the General Research Services (SGIker) of the University of the Basque Country (Spain) using a PANalytical CubiX diffractometer equipped with a copper tube, vertical goniometer, programmable slits, automatic sample exchanger, nickel filter, and PixCel detector. The measurement conditions were 40kV and 40mA, with a sweep between 5 and 70º2-theta.

Amino Acid Racemization (AAR)

Nine beds corresponding to carbonate silts and sands located in the tufa deposits (Figs. 4; 5; 6) were used for amino acid racemisation dating at the Biomolecular

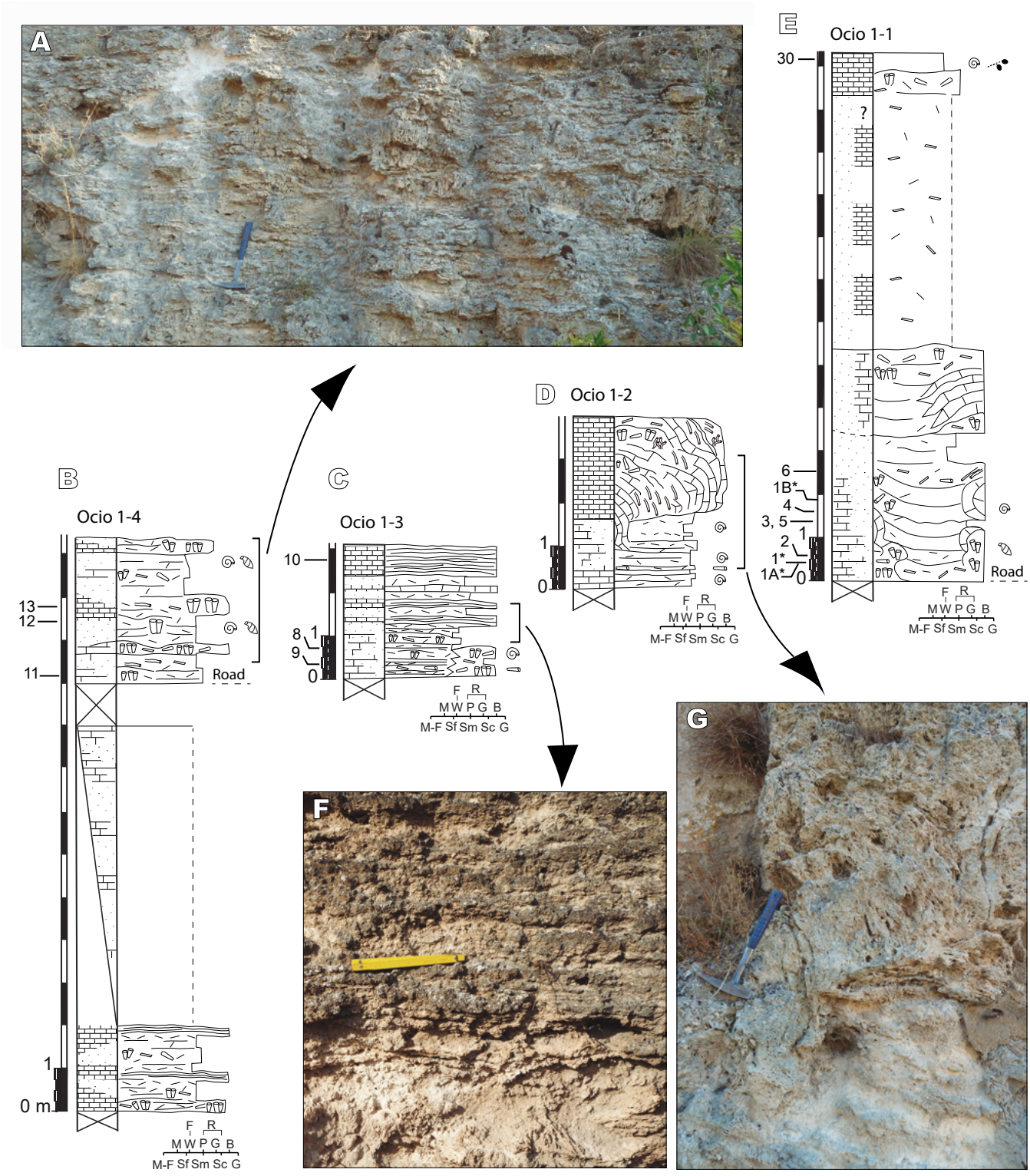

FIGURE 4. Stratigraphic sections measured in Ocio-1 (B–E) and related field images (A, F, G). A) Deposits of the upper part of Ocio, section Ocio 1-4: phytoclastic limestones (Lph, Lphf), and phytoterm tufas with vertical stems (Lst 1) interspersed with bioclastic sands (Sb). F) Deposits of the middle part of Ocio, section Ocio 1-3. Alternating stromatolite (Ls) and fine phytoclasts layers (Lphf). G) Deposits of section Ocio 1-2 consisting of alternation of bioclastic sands (Sb) and phytoclastic limestones (Lphf) at the base, and moss phytoherms (Lbr) with hanging and low-angle lying stems (Lst 2) and occasional phytoherm tufas with vertical and entwined stems (Lst 1) in the middle and upper part of section. Legend of symbols in B, C, D and E sections is in Figure 5B.

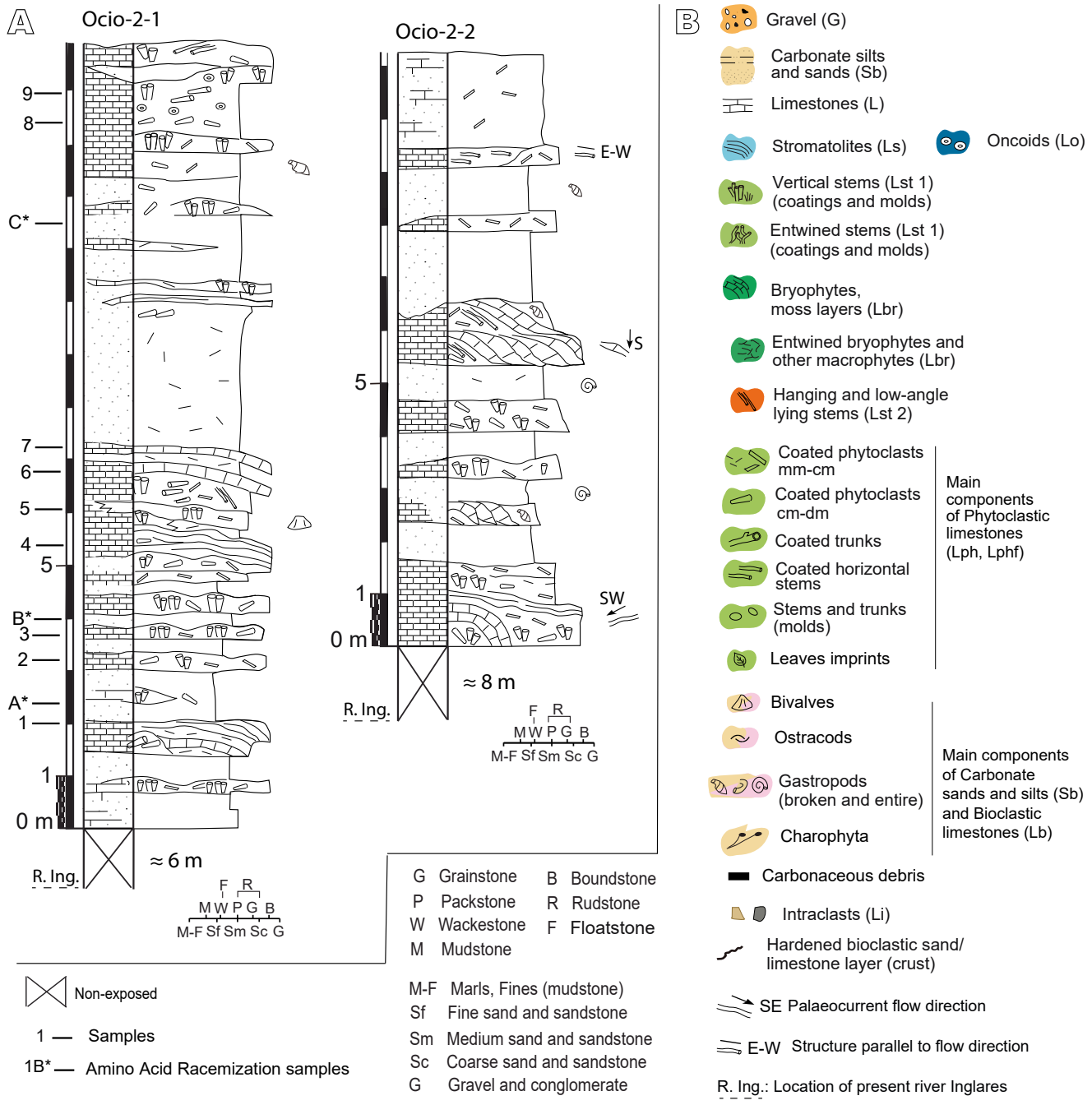

FIGURE 5. A) Stratigraphic sections measured in Ocio-2 (Ocio-2-1 and Ocio-2-2). B) Legend of symbols for Figures 4; 5A; 6; 10 and 11.

Stratigraphy Laboratory of the Universidad Politécnica de Madrid. A total of twenty-nine ostracod valves from seven beds were analysed, all of which were identified as *Herpetrocypris brevicaudata* (Table 1). The valves were carefully sonicated and cleaned with water to remove sediment. The samples were then left for 3h in hydrogen peroxide to eliminate the organic matter. Clean, translucent shells were selected from each sample. In addition, small samples near the aperture of a gastropod shell belonging to *Lymnaea* genus (Helicidae family) and a Limacidae vestigial shell were recovered from another bed (Ocio-2C, Table 1). Two opercula of the gastropod genus *Bithynia* and two valves of the bivalve genus *Pisidium* were selected from samples HER-2 and HER-6 (Fig. 6). In all cases, the peripheral parts (approximately 20–30%) were removed after chemical etching with 2N HCl. Afterward, 10–20mg of each sample was selected for amino acid racemisation analysis.

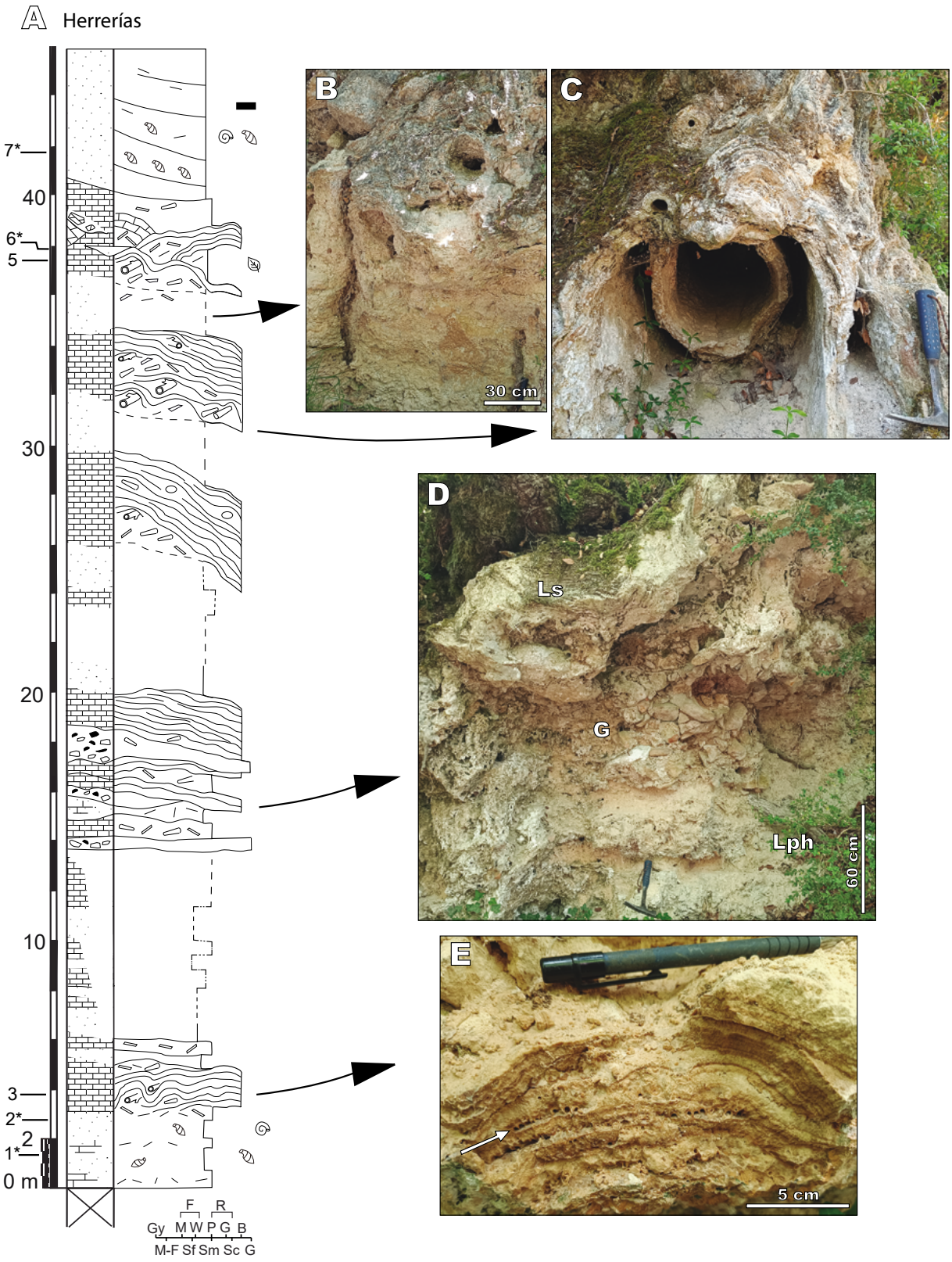

FIGURE 6. A) Stratigraphic section of Herrerías and B-E) corresponding fields images. Legend of symbols of A in Figure 5B). B) Field image of carbonate sand (Sb) and fine phytoclastic rudstone (Lpf) at the base and central part of the photograph, and phytoclastic limestones (Lph) and stromatolites (Ls) at the upper part, with leaf imprints (not visible on the image). C) Large trunk (Lph) coated by stromatolites (Ls) note several phases of stromatolite development. D) Carbonate sands (Sb) and phytoclastic limestones (Lph) at the base of the image, gravels (G) in the central part and stromatolites (Ls) at the top. E) Detailed image of stromatolites (Ls) with small rounded cavities corresponding to insect molds (arrowed).

TABLE 1. Amino Acid Racemization (AAR) results (aspartic acid (Asp), glutamic acid (Glu) D/L values) and corresponding ages. *H. brevicaudata*: *Herpetocypris brevicaudata*. MIS 1: Holocene (11.9ky to present)

Sample	Species	N	D/L Asp	D/L Glu	Age
OCIO-1	*H. brevicaudata*	4	0.358±0.019	0.124±0.007	129.0±18.1 ky
OCIO-1A	*H. brevicaudata*	2	0.365±0.006	0.134±0.001	130.9±4.5 ky
OCIO-1B	*H. brevicaudata*	7	0.347±0.011	0.104±0.011	109.5±14.3 ky
OCIO-2A	*H. brevicaudata*	5	0.183±0.007	0.029±0.003	4337.8±282.6 y
OCIO-2B	*H. brevicaudata*	1	0.127	0.022	2030.0 y
OCIO-2C	*Lymnaea* and *Limacidae*	2	0.223±0.005	0.074±0.017	5476±625 y
HER-1	*H. brevicaudata*	5	0.104±0.014	0.026±0.005	1050±120 y
HER-2	*Pisidium*	2	0.143±0.017	0.043±0.006	MIS 1
HER-6	*Bithynia*	2	0.154±0.017	0.066±0.017	MIS 1
HER-7	*H. brevicaudata*	5	0.194±0.014	0.032±0.009	4700±580 y

Amino acid concentrations were quantified using high-performance liquid chromatography following the sample preparation protocols described by Kaufman and Manley (1998) and Kaufman (2000). This procedure involves hydrolysis, which was performed under a N_2 atmosphere in HCl for 20h at 100°C. The hydrolyzates were evaporated to dryness in vacuo and then rehydrated in 7mL (ostracods) or in 10μL/mg (gastropods) of 0.01M HCl with 1.5mM sodium azide and 0.03mM L-homo-arginine (internal standard).

Samples were injected into an Agilent HPLC-1100 liquid system equipped with a fluorescence detector. The excitation and emission wavelengths were programmed at 230nm and 445nm, respectively. A Hypersil BDS C18 reverse-phase column (5μm; 250×4mm inner diameter) was used for the analysis.

To establish the numerical ages of the ostracod samples used for AAR, aspartic acid (Asp) and glutamic acid (Glu) were selected because they account for more percentage (>50%) of the amino acid content in most ostracod valves (Bright and Kaufman, 2011; Kaufman, 2000; Ortiz *et al.*, 2013). Other amino acids were excluded because of their low racemisation rates.

For dating ostracods, we applied the age calculation algorithms described by Ortiz *et al.* (2004) for samples with Asp and Glu D/L values higher than 0.27 and 0.08, respectively (OCIO-1A and OCIO-1B beds). For the ostracod-based age calculation of HER-1, HER-7, OCIO-2A and OCIO-2B beds, we used the age calculation algorithm defined by Ortiz *et al.* (2015) for samples with Asp D/L values lower than 0.30 (Holocene samples): age(y)= 17.74 D/L Asp – 0.90. In the latter case, we considered only Asp because it is an amino acid that racemises faster, and D/L Glu values cannot discriminate Holocene ages (Ortiz *et al.*, 2015).

To establish the amino acid chronology of the gastropod shells in the carbonate deposits, we also used Asp and Glu content. The mean Asp and Glu D/L values at each tufa level are shown in Table 1 along with their estimated ages. The numerical ages of the gastropod shells at the OCIO-2C and HER-6 levels were calculated by introducing Asp and Glu values into the age-calculation algorithms established by Torres *et al.* (1997) for gastropods in the central and southern parts of the Iberian Peninsula.

The age established for each bed was the average of the numerical dates obtained for each amino acid D/L value measured in molluscs or ostracods at that level, and the age uncertainty was the standard deviation of the numerical ages calculated at each level.

Palaeontological analysis

Three samples consisting of carbonate silt and sand from Ocio-1 and Ocio-2 (Ocio-1A, Ocio-2A, and Ocio-2B) were studied for their microfossil content (locations are shown in Figures 4 and 6). Each sample (approximately 1kg in weight) was sieved using <0.165mm mess light sieves. No samples were collected from the Herrerías outcrop for microfossil analysis.

C and O stable isotope analyses

Thirty-four specimens representing diverse carbonate facies from five sections (Herrerías, Ocio-1-1, Ocio-1-3, Ocio-1-4, and Ocio-2-1; sample locations in Figures 4; 5; 6) were selected to obtain pristine powder samples using a punch and microdrill for C and O stable isotope analyses. Powder from compact samples was obtained using a 0.5mm diameter micro-drill powered by a micromotor (Navfram model N120 Micromotor 25.000rpm with an electronic speed regulator, AB SHOT TECNICS SL, Cervelló, Barcelona, Spain). The device was coupled with a

stereomicroscope, which helped select rock parts showing the minimum presence of alteration, cement phases, or fossil remains. Picks from the loose and soft samples were manually taken using a stereomicroscope to avoid impurities. All samples were ground and sieved to 53μm. Powdered samples (0.2–0.5mg) were stored in glass vials.

$\delta^{13}C$ and $\delta^{18}O$ ratios were determined at the *Centres Científics i Tecnològics* of the University of Barcelona, Spain (CCIT-UB). The isotopic ratios were measured in a mass spectrometer (MAT-252, Thermo Finnigan; Thermo Fisher Scientific, Waltham, MA, USA) via CO_2 obtained in a Carbonate Kiel Device III (Thermo Finnigan) by the reaction of samples with 100% H_3PO_4 at 70ºC (McCrea, 1950). The international standards NBS-18 ($\delta^{13}C$= -5.1‰ VPDB; $\delta^{18}O$= -23.01‰ VPDB) and IAEA-603 ($\delta^{13}C$= 2.46‰; $\delta^{18}O$= – 2.37‰ VPDB), and internal RC-1 ($\delta^{13}C$= 2.78‰ VPDB; $\delta^{18}O$= -2.08‰ VPDB) were used. The overall reproducibility was greater than 0.02‰ for both $\delta^{13}C$ and $\delta^{18}O$. The results are reported in δ ‰ notation relative to Vienna Pee Dee Belemnite (VPDB) (Table 2).

RESULTS

Chronology: Amino acid racemization ages

The age results of the AAR analysis are listed in Table 1. In the case of HER-6, no numerical age could be stated, and it was set within MIS 1. No algorithm has been established for *Pisidium*; however, by comparing Asp and Glu D/L values, the resulting age fits well within MIS 1. The mean Asp and Glu D/L values of the ostracod valves of the beds are shown in Table 1. Of the ostracod samples, two results from OCIO-1B were excluded because the Asp and Glu D/L values fell off the covariance trend (cf. Kaufman, 2003, 2006; Laabs and Kaufman, 2003) and/or because of abnormally high D/L values, characterised by Asp D/L and Glu D/L values falling outside the 2σ range of the group (cf. Hearty *et al.*, 2004; Kosnik and Kaufman, 2008).

Ocio-1 samples yielded Middle–Late Pleistocene ages: OCIO-1 is 129.0±18.1ky; OCIO-1A is 130.0±4.5ky and OCIO-1B is 109.5±14.3Ky, within the MIS 5 (*i.e.* MIS 5e (Eemian)). Ocio-2 samples provided Holocene ages: OCIO-2A was dated at 4,377.8±282y, OCIO-2B at 2,030.0y, and OCIO-2C at 5,476±625y, all of which fit the MIS 1 age. Samples HER-1 and HER-7 also yielded Holocene ages: HER-1 is 1,050±120y, and HER-7 is 4,700±580y. HER-2 and HER-6 were set at MIS 1. These AAR Holocene ages are not fully in accordance with the stratigraphic position of the corresponding samples (Figs. 5; 6); that is, OCIO-2C is ≈7.2m over OCIO-2B and ≈9m over OCIO-2A. Likewise, HER-7 is at the top of the stratigraphic section. However, despite the discrepancies among the Holocene data, the overall set of AAR data allowed the separation of two groups of tufa deposits based on their AAR ages: MIS 5 (Ocio-1) and MIS 1 (Ocio-2 and Her).

Palaeontological content

The samples collected from Ocio-1 yielded greater microfossil diversity than those collected from Ocio-2. The macrofossils determined in the Ocio-1 samples included well-preserved gyrogonites such as those of *Chara* cf. *hispida*, abundant specimens of three aquatic gastropod species (*Amullaceana* cf. *balthica*, *Bithynia tentaculata* and *Planorbis planorbis)* and seven species of ostracods (the most abundant being *Herpetocypris brevicaudata, Paralimnocythere psammophila, Pseudocandon eremita and Ilyocypris gibba)* (Fig. 7). In Ocio-2, only a

TABLE 2. $\delta^{13}C$ and $\delta^{13}O$ values of the analysed carbonate samples, with indication of sedimentary facies. All samples consisted of calcite (100%), as indicated by the XRD analyses

Sample	Sedimentary facies	$\delta^{13}C$ (VPDB‰)	$\delta^{18}O$ (VPDB‰)
OCIO1-1	Sb	-8.28	-7.50
OCIO1-2	Lst1	-8.38	-6.76
OCIO1-3	Lbr	-8.38	-7.20
OCIO1-4	Lb	-8.26	-7.27
OCIO1-5	Lb	-8.41	-6.40
OCIO1-6	Lph	-8.48	-7.33
OCIO1-7	Lph horiz	-8.38	-7.08
OCIO1-8	Lst1	-8.69	-7.44
OCIO1-9	Lst1	-8.63	-7.36
OCIO1-10	Ls	-8.19	-7.16
OCIO1-11	Lst1	-8.22	-7.18
OCIO1-12	Lst1	-8.84	-7.60
OCIO1-13	Lphf	-8.37	-7.54
OCIO1-14	Lphf	-8.19	-7.29
OCIO1-15	Ls	-8.18	-7.64
OCIO1-1B	Sb	-8.17	-7.57
OCIO2-A	Sb	-7.80	-6.98
OCIO2-B	Sb	-7.40	-7.23
OCIO2-C	Sb	-7.91	-7.16
OCIO2-1	Ls	-7.54	-7.65
OCIO2-2	Lst1	-7.30	-7.03
OCIO2-3	Lph. Lphf	-7.21	-6.94
OCIO2-4	Ls	-7.64	-8.00
OCIO2-5	Lph-Lst1	-7.67	-6.87
OCIO2-6	Lbr	-8.12	-7.72
OCIO2-7	Lbr	-7.97	-7.00
OCIO2-9A	Lo	-7.89	-7.34
OCIO2-9B	Lo	-8.16	-7.45
HER-1	Sb	-8.31	-7.65
HER-2	Sb	-9.01	-7.39
HER-3	Ls	-8.79	-8.55
HER-5	Ls	-9.14	-8.59
HER-6	Sb	-8.58	-7.33
HER-7	Sb	-7.24	-8.17
Average±St. deviation		-8.17±0.49	-7.39±0.46
Correlation coefficient (r)		0.24	

few fragments of two species of ostracods (*Herpetocypris brevicaudata* and *Pseudocandon parallela*) and a few individuals of the terrestrial gastropod *Helicella ordunensis* occur. In the Herrerías area the sediment samples were not water-screened for microfossil study; however, the same three species of gastropods present in Ocio-1 could be identified, based on visual inspection (Larena *et al.*, 2025).

Stratigraphy

Tufa outcropping deposits are irregularly distributed along the Inglares River Valley (Figs. 2; 3). Sections measured in Ocio-1 and Ocio-2 (that is at the El Tobal zone, 0.8km to the West and Southwest of the Ocio locality) yielded a composite thickness of approximately 25m and 15m, respectively (Figs. 4; 5). The thickest outcropping deposits (approximately 45–50m thick) occur upstream of Berganzo in the most upstream zone of the *Water route*. The Herrerías section was measured along a path that provided access to the Herrerías waterfall. However, outcrop conditions prevented the measurement of a complete record (Fig. 6).

These deposits consist of various carbonate facies (both indurated and made of loose fine-grained sediment; all of them composed solely of calcite), and minor interbedded gravel (consisting of extraclasts from Cretaceous–Paleocene carbonate rocks). Carbonaceous debris is a rare component observed only in the Herrerías section (Table I, see Appendix). Figures 4–6 present seven stratigraphic-sedimentological sections measured at El Tobal and Herrerías and Figures 8–11 show field images with some noticeable sedimentological characteristics.

The basal contact of the studied Quaternary tufa with the underlying substrate is only visible in the upper portion of the Herrerías section, where tufa deposits lie unconformably over the Cretaceous and Palaeocene carbonate rocks. Discontinuous gravel deposits occur in this section, which likely correspond to hillside fall deposits. Contact between the oldest tufa and the substrate is not visible elsewhere; thus, thickness measurements from the outcropping deposits represent the minimum estimates of the total tufa thickness. The contact between Pleistocene and Holocene deposits in the Ocio remains unclear (Fig. 2B).

In addition to these outcrops, some flat areas on or close to the present floodplains, such as around the Peñacerrada locality (segment A, Fig. 3), between the Ocio and Berganzo localities (segment C, Fig. 3), and to the West of the Ocio locality (segment D; Figs. 2; 3), were surveyed. Despite their poor preservation and exposure due to agricultural uses, they all consist of whitish, light greyish, and cream-coloured fine-grained, mostly sand-size, loose carbonate

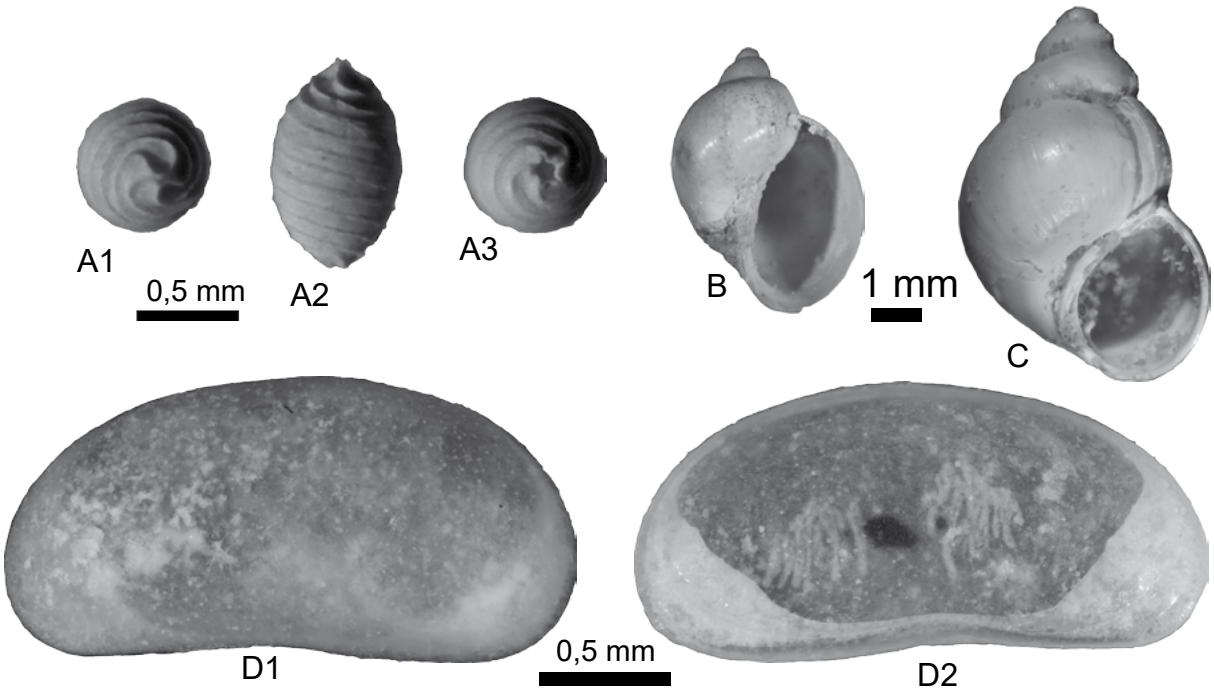

FIGURE 7. Fossil assemblage of Ocio 1. A) Gyrogonite of *Chara* cf. *hispida*. A1) Apical view; A2) Lateral view; A3) Basal view. B) *Amullaceana* cf. *balthica*. C) *Bithynia tentaculata*. D) *Herpetocypris brevicaudata*. D1) External view; D2) Internal view.

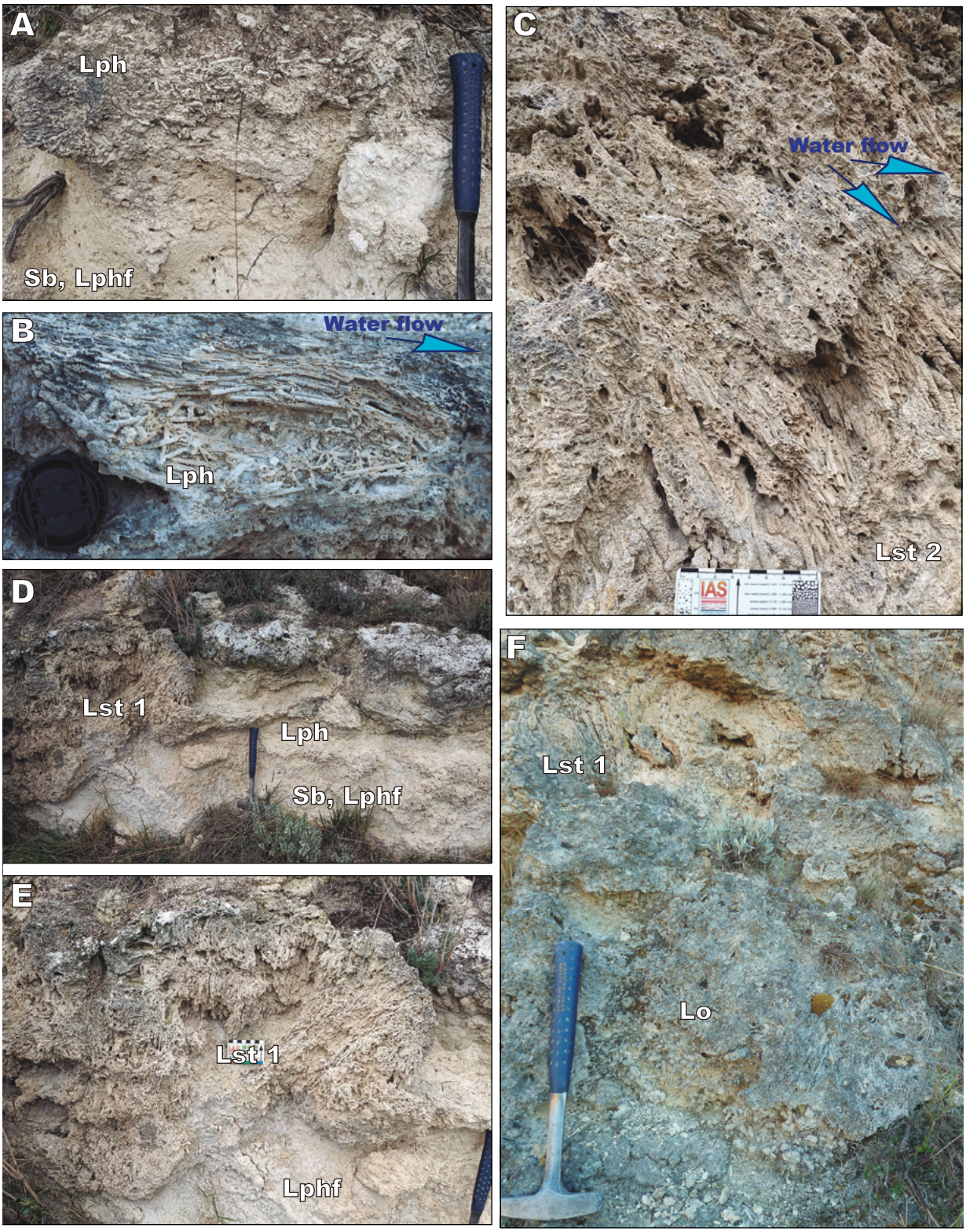

FIGURE 8. Field images of different facies. A) Carbonate sand (Sb) and fine phythoclastic limestone (Lphf) overlied by phytoclastic rudstone (Lph). B) Detailed of phytoclastic rudstone-boundstone (Lph) consisting of calcite coated stems, randomly oriented and parallel oriented over a subhorizontal surface, indicating the water flow direction. C) Detail of a phytoherm boundstone, showing curtains of down-growing stems over a highly inclined surface (Lst 2). D) Stem boundstone (Lst 1) passing laterally to carbonate sand (Sb) and fine phytoclastic rudstone (Lphf), with increasing phytoclast size and proportion toward the top (Lph). E) Detail of D showing stacked up-growing stems forming small barrage (Lst 1). F) Oncoidal rudstone (Lo) and phytoherm boundstone consisting of stems (Lst 1) at the top.

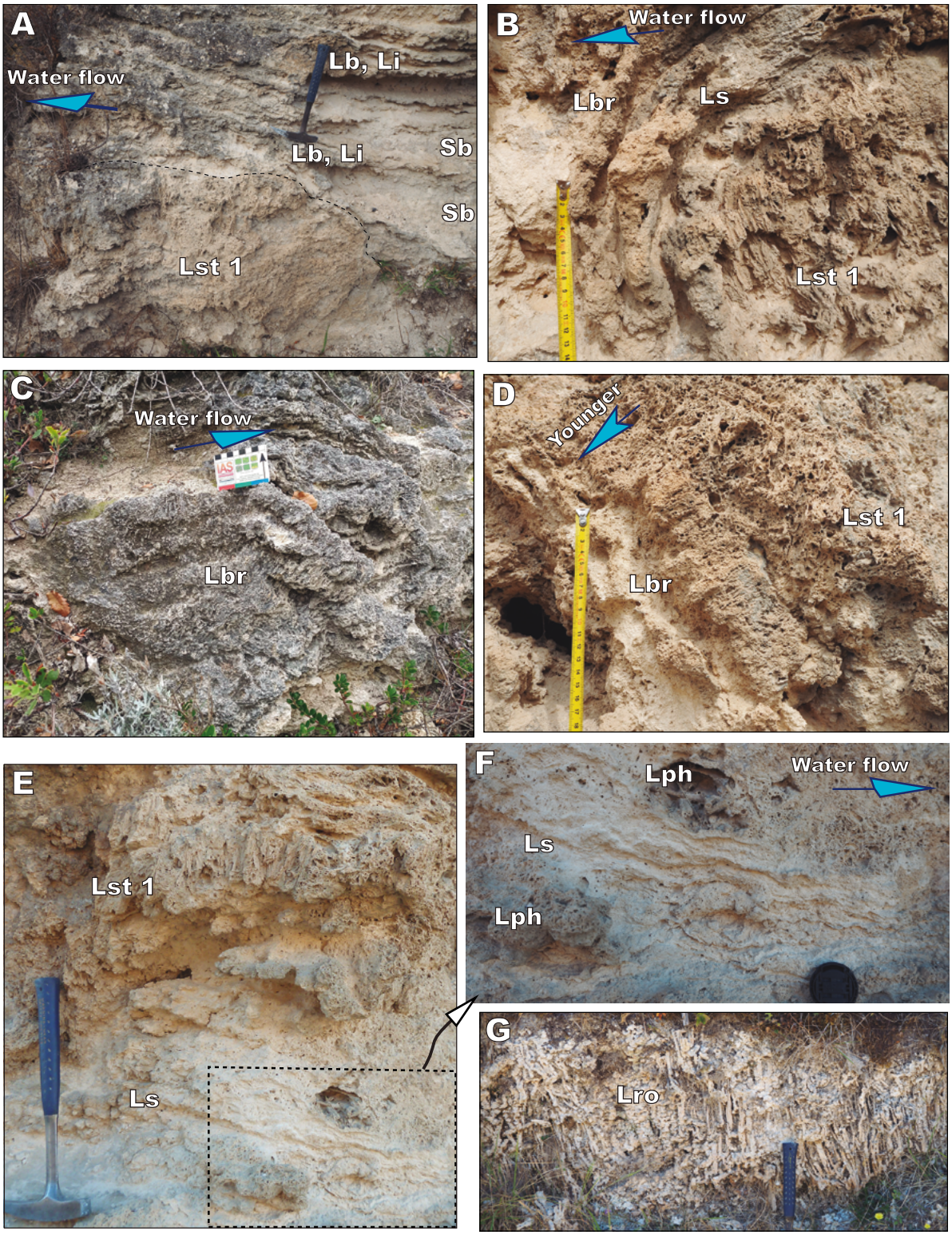

FIGURE 9. A) Phytoherm formed of upgrowing vertical stems (Lst 1), partially forming of a small barrage. Carbonate sands (Sb), bioclastic (Lb) and/or intraclastic wackestone-packstone (Li) layers represent deposition in partially dammed water areas. B) Subvertical upgrowing stems (Lst 1), coated by stromatolitic limestone (Ls) and bryophyte limestone (Lbr). The growth of bryophytes indicates the direction of the water flow. C) Bryophyte boundstone (Lbr). D) Detail of a phytoherm boundstones consisting of intertwined stems (Lst 1) and bryophyte boundstone (Lbr), showing the growth direction. E) Stromatolitic limestone (Ls) at the base and phytoherm boundstones consisting of vertical stems and other with non-oriented stems (Lst 1). F) Detailed of E. The orientation of the stems of the Lph facies and dip of Ls layers indicate the water flow direction. G) Vertical oriented, centimetric long roots, calcrete (Lro).

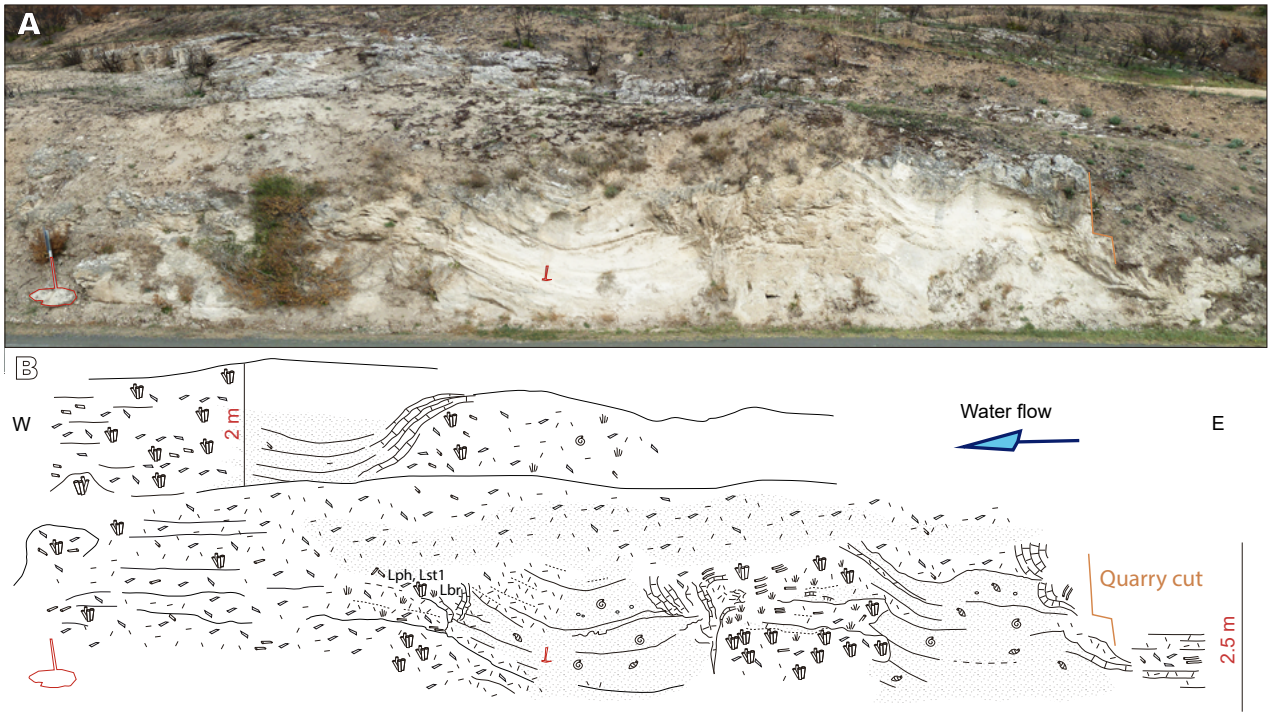

FIGURE 10. A) Field image of Ocio-1 deposits, where section 1-1 was measured. B) Drawing from A showing facies and geometry of deposits. Explanation in the text. Legend of symbols in Figure 5B.

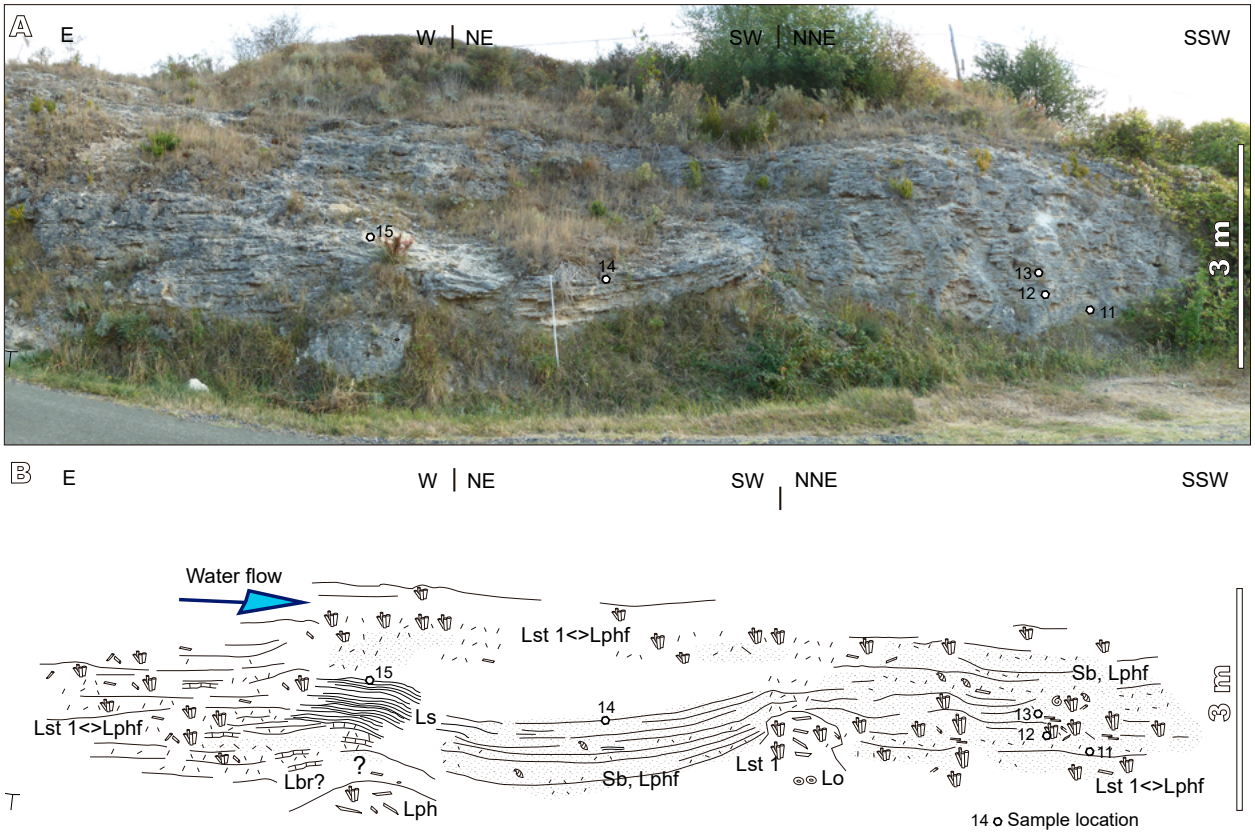

FIGURE 11. A) Field image of Ocio-1 deposits. B) Drawing from A, showing facies and geometry of deposits. Numbers correspond to samples. Explanation in the text. Legend of symbols in Figure 5B.

sediments, which primarily correspond to unindurated tufa deposits (*e.g.* facies Sb, Table I). Information provided by the inhabitants of the Ocio locality (shallow ditches for housing and street work) allows to infer that this locality is settled on loose and poorly consolidated tufa and alluvial deposits, as well as on the composition of the surrounding flat areas. Based on the aforementioned information and AAR ages obtained in this study, the following chronological groups are tentatively proposed (Table 1; Fig. 2A, B):

Middle and Late Pleistocene: the deposits of this group correspond to the outcrop located 0.8km to the West of the Ocio locality (Ocio-1), where ages provided by the AAR (Table 1) fit MIS 5 (Fig. 4).

Middle and Late Holocene: the deposits of this group include the outcrops located at Ocio-2 and those located East of Berganzo over the Herrerías waterfall, where the AAR ages (Table 1) fit MIS 1 (Figs. 5; 6).

Quaternary to recent alluvial and loose tufa deposits. These comprise fine-sized polygenic alluvial deposits and loose sand-silt-sized detrital tufa that occupy some flat areas located upstream and downstream of the Ocio-1 deposits and also occur upstream of the Herrerías site (Fig. 3). However, the precise ages remain unknown. It was first established in the Holocene by Portero *et al.* (1979). However, some of these could be Middle–Late Pleistocene in age, based on the surface continuity between them and the Ocio-1 deposits, suggesting a lateral relationship.

Sedimentology

Sedimentary facies

Up to eleven carbonate facies and one detrital facies (extraclastic gravel) were differentiated in the studied tufa deposits based on lithology and physical and biological attributes (Table I). They are mainly distinguished according to features such as bed geometry and continuity, texture, sedimentary structures, and biological constituents. The descriptions and depositional interpretations are presented in Table I. All carbonate facies consist of calcite, as determined by XRD and microscopic analyses. No separation by area or age was made when determining and describing the facies types because there were no significant differences in their characteristics among the different studied areas.

The most abundant facies are phytoclastic rudstones (Lph; if fine phytoclasts, Lphf), bioclastic carbonate sand and silt (Sb), and up-growing stem boundstones or stem phytoherms (Lst 1), followed by stromatolites (Ls). Other less abundant facies types are bryophyte boundstones or moss phytoherms (Lbr). Oncoid rudstones (Lo), bioclastic limestones (Lb), and downgrowing stem boundstones (Lst 2) are less common, whereas intraclastic packstones (Li), root boundstones (Lro), and gravel (G) are rare. In the field, the geometry of the deposits in cross-section (2D) varies depending on the facies type: lenticular and tabular (*e.g.* bodies consisting of Lph, Lphf, Sb, and Ls), lenticular (*e.g.* Lst 1, Lb, Lo, Lro, and Li), hemi-domal, and lenticular (*e.g.* Lbr and Lst 2). Commonly, these facies change laterally and vertically, and their thickness and continuity are highly variable (Table I; Figs. 8; 9; 10; 11).

Most calcite coatings on plant stems form facies Lst 1, Lst 2, and Lph, consisting of submillimetre- to a few millimetre-thick successive laminae formed of micrite and microspar to spar calcite. Some empty trunks molds with 10 to 30cm long inner diameters exhibit up to 18cm thick laminated thickness (Fig. 6C). Only a few structureless coatings were observed. The laminae contain evidence of microbes; both calcite tubes and filament moulds from filamentous microbes (likely cyanobacteria) are preserved, commonly forming fan- and bush-shaped bodies (Fig. 12A, B, C). Stromatolites, at places developed over ground trunks and stems, and oncolites consist of submillimeter to 2mm-thick laminae formed of micrite to microspar calcite, which results from the vertical stacking of successive delicate structures consisting of laterally grouped calcite-coated filaments (*i.e.* tubes), the height of which can equal the lamina thickness (Fig. 12D, E, F, G). The inner diameter of the tubes ranges from 2 to 10μm, matching small filamentous cyanobacteria (Fig. 12G, H) or perhaps some filamentous algae. Some laminated coatings consist of large blade-shaped crystals that form continuous palisades and contain less evident microbial filaments.

Bryophyte boundstones (Lbr) consist of stacked bands that are a few to four centimeters thick. Within each band, calcified moss caulidia and filidia, which are preserved empty moulds, are set perpendicularly to the accumulation surface (Fig. 13A–C). Carbonate sands and silts (Sb) contain diverse gastropods, ostracods, charophyte gyrogonites, and non-skeletal carbonate grains such as clots of calcite crystals (Figs. 7A; 13D, E). Bioclastic mudstones and wackestones (Lb) consist of bioclasts *s.l.*, among which there are sparse charophytes (*e.g.* stems; Fig. 13F). A few compact limestone layers up to 10cm thick contain abundant heterometric intraclasts (Li; Fig. 13G).

The porosities of the different facies display interparticle, growth framework, and mouldic types. Generally, porosity is high (up to 20%). Macroscopic porosity is conspicuous in facies Lph, Sb, Lst 1 and Lbr. Microscopic porosity is larger in the majority of laminated structures (*e.g.* facies Ls and Lo) than in the rest of the facies. Post-sedimentary features are limited to partial filling with calcite in some interparticle pores. No distinct recrystallisation has been

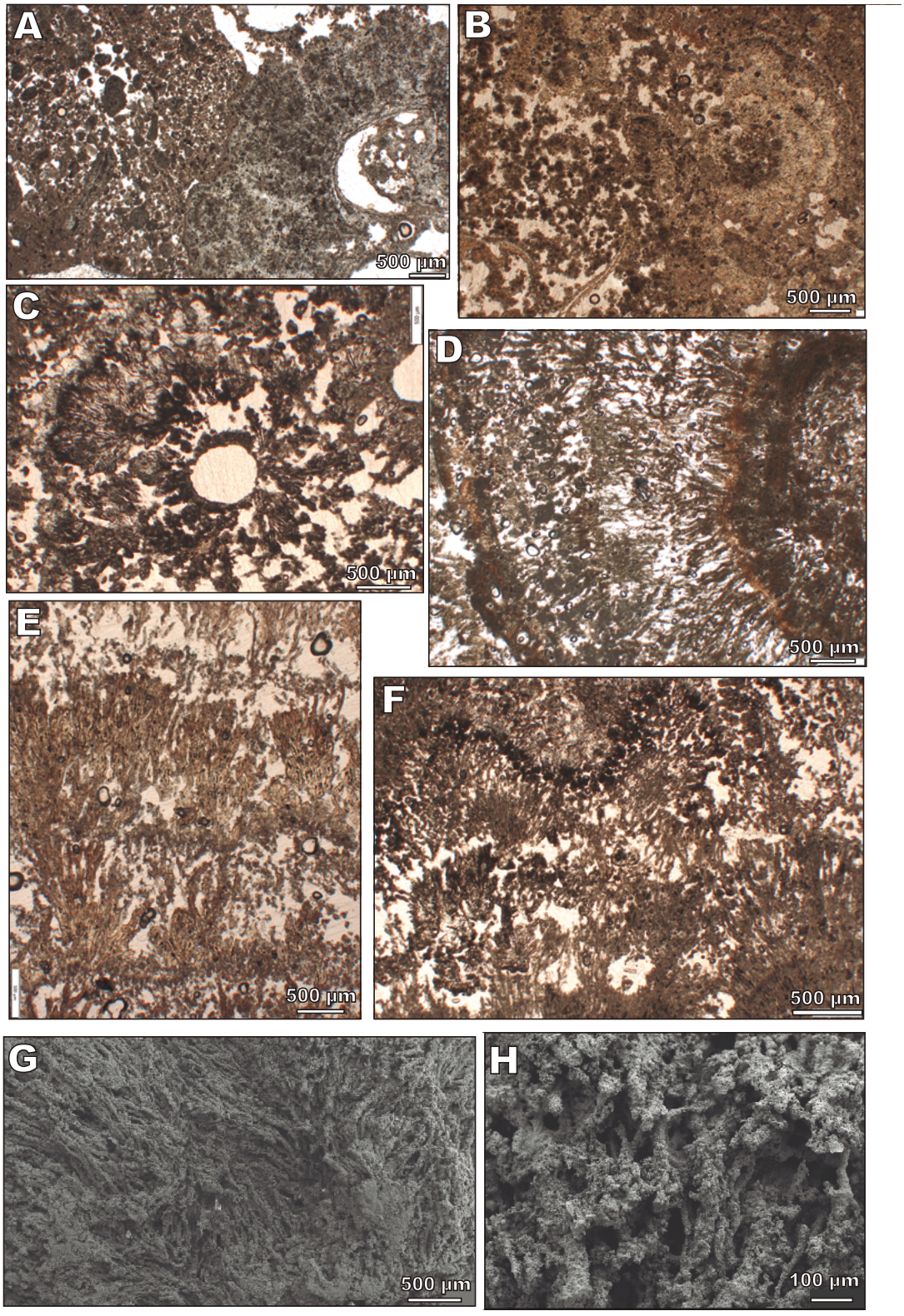

FIGURE 12. Optical (A–F) and Scanning Electron Microscope (G, H) photographs of tufa facies. A) Cross-section of a coated stem surrounded by intraclast rudstone. Note lamination in the stem coating. B) Cross-section of an in situ coated stem surrounded by clotted micrite. Note lamination in the outer part of stem coating. C) Cross-section of fine stem coated by bush-shaped bodies representing microbial bodies. D) Oncoid section showing successive laminae formed of micrite filaments representing microbial bodies. E) Laminae consisting of microbial filaments in stromatolite. Note laminae formed of diverse crystal sizes. F) Ondulate lamination formed of adjacent bush-shaped bodies consisting of microbial filaments. G) and H) Calcite tubes formed by calcite precipitation on filamentous microbes, producing lamination of oncoids.

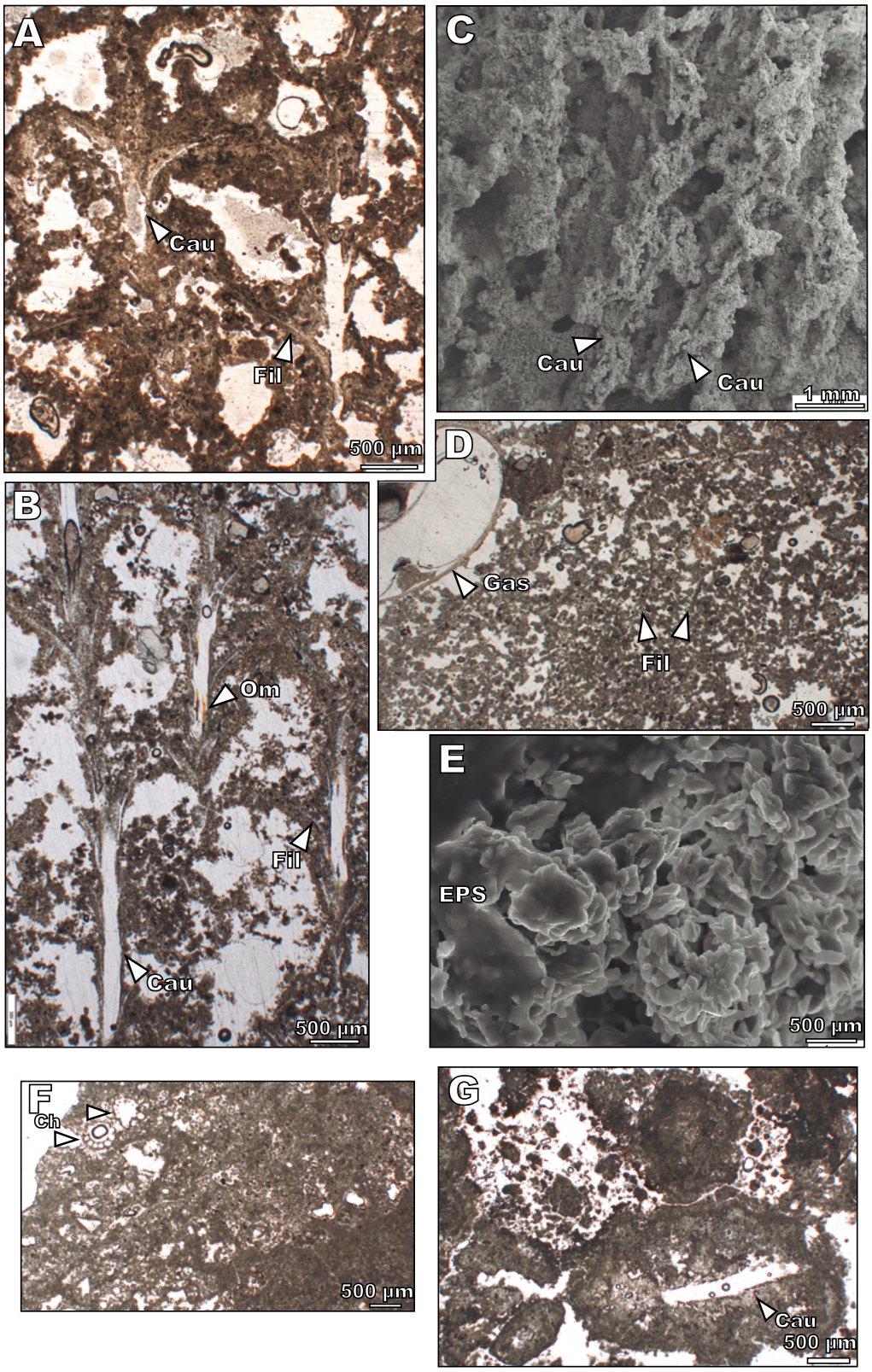

FIGURE 13. Optical (A, B, D, F, G) and Scanning Electron Microscope (C, E) photographs of tufa facies. A) and B) Moss boundstone. Note high porosity, preservation of empty caulidia (Cau) and filidia (Fi), and organic matter (Om). C) Moss boundstone showing varied crystal sizes forming the moss coatings. D) and E) Carbonate sand and silt (Sb). Note in D gastropod (Gas) and filaments (Fil), and in E, mucilaginous substance (EPS) and filaments. F) Bioclastic wackestone (Lb). Note sections of charophyte thali (Ch). G) Intraclastic limestone. Note intraclast containing moss caulidia (Cau).

observed, except in a few stromatolite laminae in Herrerías, where elongated spar calcite crystals set perpendicular to lamination occur.

C and O stable isotope composition

The $\delta^{13}C$ and $\delta^{18}O$ values of the analysed samples range from -7.21 to -9.14‰ VPDB, and from -6.40 to -8.59‰ VPDB, respectively. The average values are: $\delta^{13}C$= -8.17±0.49‰ VPDB and $\delta^{18}O$= -7.39±0.46‰ VPDB (Table 2; Fig. 14). There was no consistent isotopic distinction among the different facies; in many cases, the limited number of samples per facies made significant comparisons more difficult (Table 3). With regard to age, the samples of Ocio-1 and Ocio-2 are set apart by the $\delta^{13}C$ values, with very little overlapping between these two sample groups; the average $\delta^{13}C$ is 0.66‰ higher in the Holocene (Ocio-2) than in the Pleistocene deposits (Ocio-1) (Fig. 14). The average $\delta^{18}O$ values for the two groups are almost identical. The Herrerías samples partially overlap these two groups and display the lowest average $\delta^{13}C$ and $\delta^{18}O$ values (Fig. 14; Table 3). The correlation coefficient (r) between $\delta^{13}C$ and $\delta^{18}O$ is poor for all data combinations.

INTERPRETATION AND DISCUSSION

Characteristics of the fluvial sedimentary environment

The sedimentary facies characterised in this study (Table I) have been described in many other tufa-bearing systems (*e.g.* Arenas *et al.*, 2000; Arenas-Abad *et al.*, 2010; Azennoud *et al.*, 2021; Capezzuoli *et al.*, 2009; Fernandes *et al.*, 2023; Ordóñez *et al.*, 2016; Pedley, 1990, 2009; Rodríguez-Berriguete *et al.*, 2018, 2021; Sallam, 2022; Vázquez-Urbez *et al.*, 2012; Violante *et al.*, 1994, among others). The aforementioned facies are arranged into simple vertical sequences (or Facies Associations, FA) that record the sedimentary processes that occurred in a particular sedimentation area through time as a result of progradation, aggradation, retrogradation or abandonment of the sedimentary subenvironments (lithotopes) in a fluvial system through time (Arenas-Abad *et al.*, 2010). Four main FA representing diverse subenvironments were distinguished (Fig. 15): FA 1) barrages, cascades, and dammed areas; FA 2) shallow barrage (without cascades) and dammed areas; FA 3) low-slope channel (without cascades) and FA 4) palustrine zones in dammed areas and floodplains.

FA 1 represents the development of cascades, barrages, and pools at diverse scales along the river course. Three possible scenarios were identified.

FA 1a: Barrage-cascade and dammed area. This FA results from prograding-aggrading cascades associated with barrages, which dam water upstream. Barrages resulted from phytoherm and phytoclast accumulation (facies Lst 1 and Lph) along some areas of the channel (Fig. 9A). Moss mats (facies Lbr) and microbial mats (facies Ls) developed on the top and downstream portions of some barrages (Fig. 9B, C), producing variably increasing barrage sizes. Down-growing plants lying parallel to the flow (Lst 2) were associated with these facies (*e.g.* at the base and middle parts of Ocio-1-2; Fig. 5B). The progradation and aggradation of this structure, principally by moss-layer stacking, increased the height of the cascade front, favouring the damming of water upstream. In the pooled areas, a diversity of components formed and accumulated: lime mud, submillimetre fragments of previously fragile tufa deposits (*e.g.* calcite-coated moss and microbialite layers), fine-sized bioclastic sediments, including shells of ostracods and gastropods (facies Sb, Lphf and Lb; Fig. 7), and minor intraclasts and small oncoids (facies Li and Lo). Charophyte stems and gyrogonites were preserved in facies Sb and Lb (Figs. 7; 13F), indicating the growth of charophyte meadows in the pools. Horizontal lamination and banding in these fine deposits reflect changes in the water flow conditions. Downstream, the barrage-cascade structures were laterally related to pools with dominant fine phytoclasts (Lphf). The shallow parts of the dammed areas could be colonised by up-growing hydrophilous plants, the submerged parts of which would be coated with calcite (facies Lst 1). The lower sections of Ocio-1-1 (Fig. 4E) and Ocio-2-2 (Fig. 5B) contained representative examples of the development of this association.

FA 1b: Vertical cascade over the downstream dammed areas (without barrages). This FA corresponds mostly to prograding cascades over water-pooled areas without damming the water upstream (as reflected by its final configuration). This situation resulted from highly inclined surfaces, producing almost vertical waterfalls coated by moss, rare microbial mats, and hanging plants (Lbr, Ls and Lst 2), which mainly grew downward. The cascades hung on slow-flowing pooled water zones in which facies Lphf, Sb, and Lb formed. The upper parts of the cascades could have been partially eroded during increasing flow episodes and eventually colonised by up-growing plants (Lst 1). This FA was recognised in the eastern portion of the outcrop Ocio-1-2 (Figs. 4D, G; 8C).

FA 1a and 1b are typical of gently steep stretches associated with dammed areas along stepped fluvial systems (Arenas-Abad *et al.*, 2010) and represent the occurrence of small knickpoints along the valley (*e.g.* Gradziński *et al.*, 2013; Pedley, 2009; Vázquez-Urbez *et al.*, 2012). Both associations have also been recognised in other Quaternary fluvial systems such as southern Italy (Violante *et al.*, 1994), western Turkey (Toker, 2017), northeastern Spain (Arenas-Abad *et al.*, 2010; Arenas *et al.*, 2014b; Vázquez-

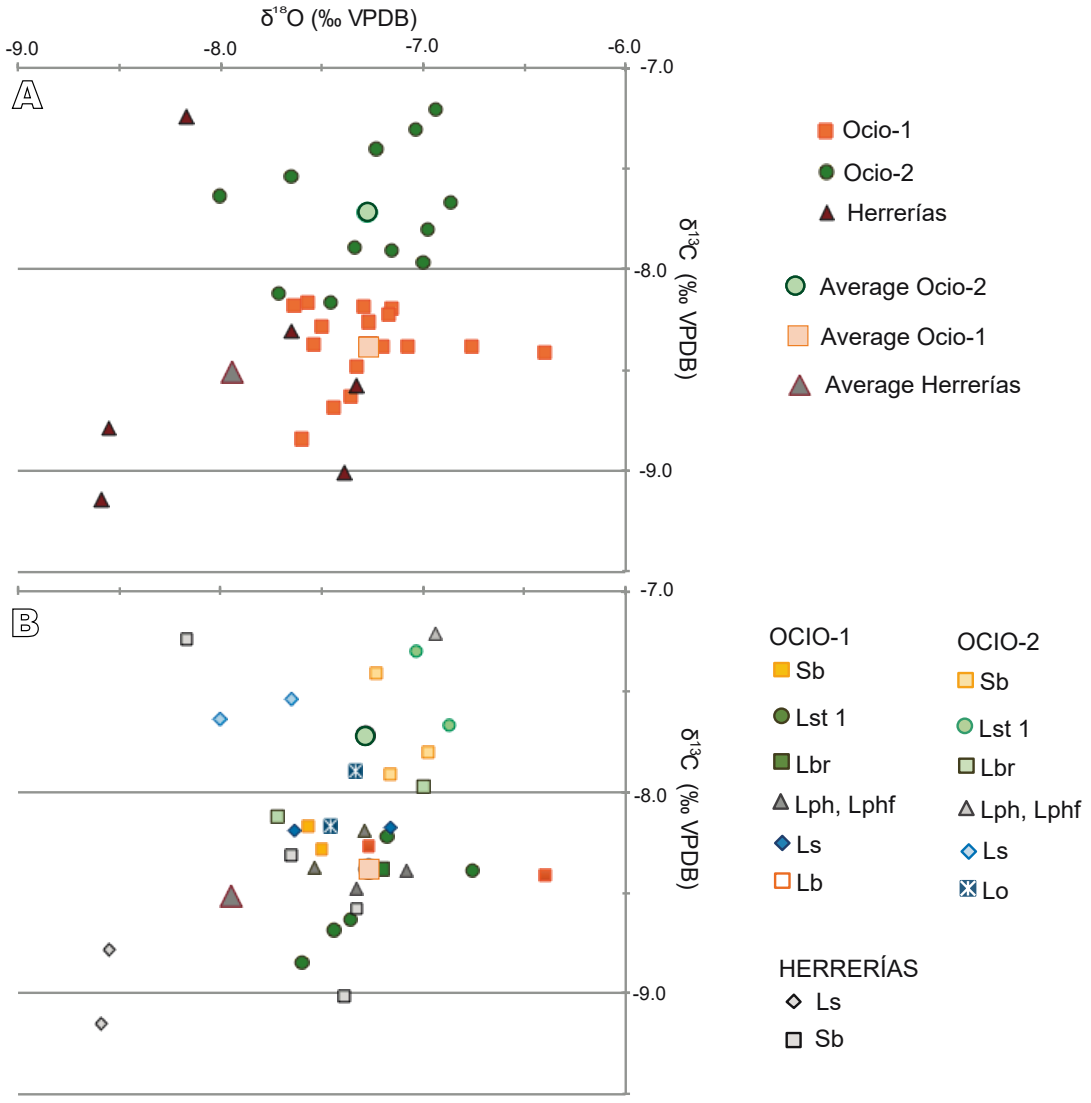

FIGURE 14. A) $\delta^{13}C$ versus $\delta^{18}O$ (‰ VPDB) of the studied three groups. B) $\delta^{13}C$ versus $\delta^{18}O$ (‰ VPDB) of the studied three groups, according to facies types. Values in Table 2.

Urbez *et al.*, 2012) and central Portugal (Fernandes *et al.*, 2023).

FA 1c: Steep stepped cascade (with small, dammed areas). This FA formed in highly inclined zones along the riverbed with stepped cascades and small water pools. High flow and unstable hillsides favoured bedrock erosion and disruption of vegetated areas, causing gravel, stems, and trunks to accumulate in high to moderate slope areas along the riverbed (that is, facies G and Lph in stepped cascades). Some trunks and stems were entirely coated with microbial mats. Once grounded, both coated and uncoated trunks and stems were sites for further growth of microbial mats, producing undulating facies Ls (Fig. 6C, E). Small pools could form in the less steep portions downstream, where mostly fine-grained carbonate sediment accumulated (facies Sb), but larger particles could also reach these areas (Lph). Rare moss-mound bodies formed during or at places of low flow conditions. This sequence mostly reflects the aggradation in high-slope stepped cascades with small pools between them. The final stages correspond to extensive deposition in backdammed areas, suggesting the downstream development of barrage cascades that overpass the height of the upstream structures. Notably, FA 1c was only recognised in the Herrerías zone, which is characterised by the steepest river gradients in the study area (Fig. 3).

This type of high-slope cascade with dominant stromatolites was described by Violante *et al.* (1994) in the Quaternary tufas of central Italy. In the Pleistocene deposits of the Añamaza River valley, stromatolite and moss

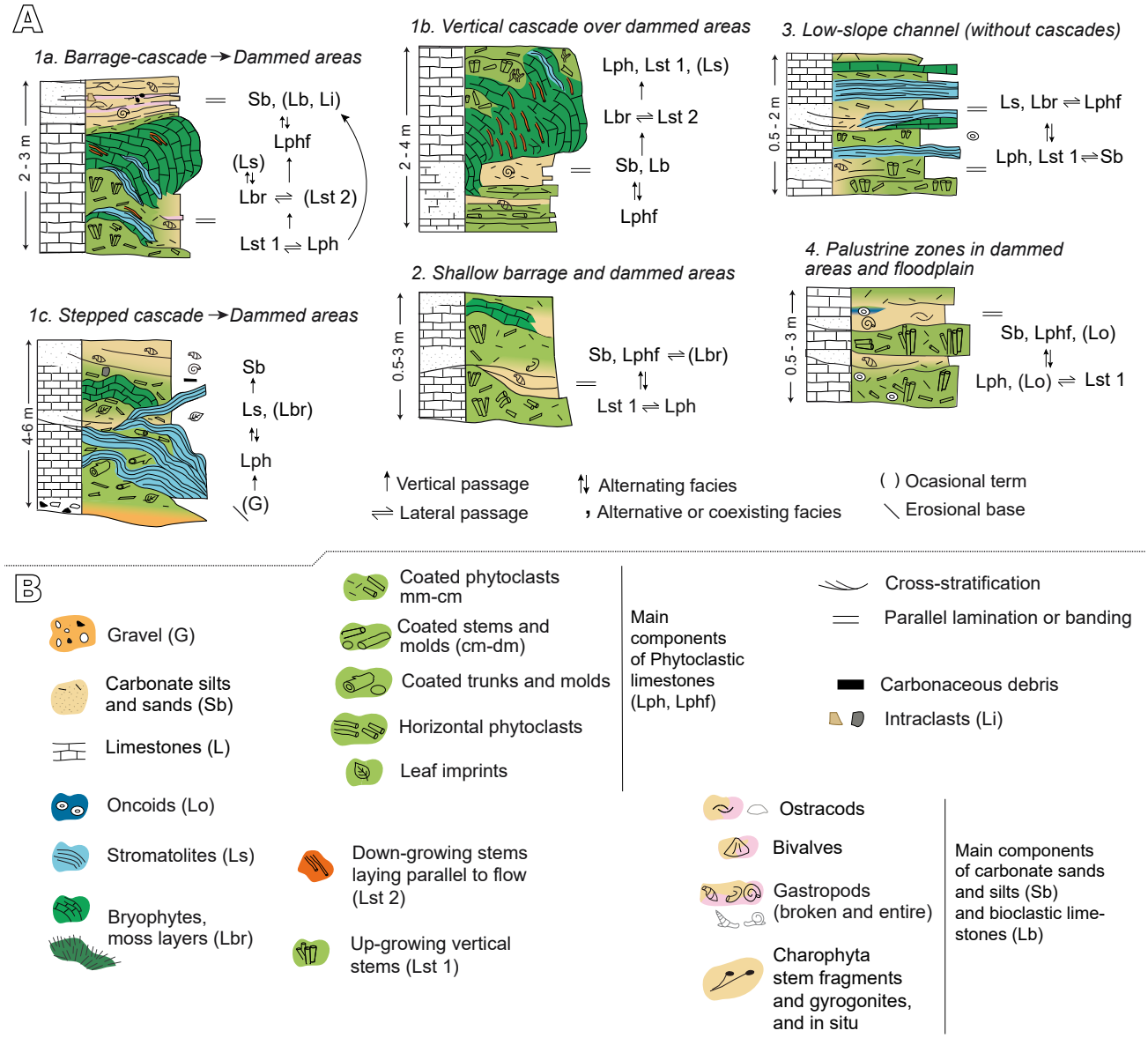

FIGURE 15. A) Vertical associations of sedimentary facies (FA 1 to FA 4). Explanation in text. B) Key notes and symbols for Figures 15A and 16.

bioherms that formed in stepped cascades were associated with gravel (facies G) and facies Lph (including trunks) and were bounded by erosional surfaces, denoting episodes of vigorous erosional processes (Arenas *et al.*, 2014b).

FA 2 represents shallow barrages and dammed areas without cascade development. Barrages were formed mainly by the accumulation of plant phytoherms (Lst 1) that could hold water between them. Locally, the downstream side of the barrage could be colonised by moss mats (2–4cm-thick moss layers) without the development of cascades, generally producing thin Lbr deposits. Shallow pools with slow-flowing water were sites where ostracods and gastropods lived, and fine-grained carbonate sediment accumulated (facies Sb, Lphf) (Fig. 9A) and even desiccated, causing in situ brecciation and hardening (facies Lb and Li). The filling ends with plant colonisation (facies Lst 1) and/or the deposition of phytoclasts (Lph, Lphf). FA 2 recorded the filling of shallow pools between small barrages along the low-slope stretch of the riverbed, principally by aggradation. This FA was detected in the eastern part of Ocio-1 (Figs. 9A; 10). A similar situation has been observed in some Pleistocene deposits of the Piedra River (Vázquez-Urbez *et al.*, 2012).

FA 3 reflects the deposition in low-slope channel zones without cascades or significant jumps, as evidenced by the geometry of the depositional bodies. Plant phytoherms

(facies Lst 1) that formed in shallow water and already had their submerged parts coated by calcite could be partially broken during increases in flow strength, and their fragments accumulated nearby (facies Lph), both in free-flowing water areas and small and shallow pools, as Lphf, along with facies Sb. This situation alternated with the development of microbial mats and moss mats, generally on extensive low-slope areas and without forming cascades, for example on gentle ramps and rapids and on the margins of some short barrages. In the latter situation, facies Ls and Lbr passed laterally into the pool facies, that is, facies Sb and Lphf. Thus, FA 3 records changes in flow conditions along low-slope stretches of the river course that led to the formation of facies Lph during periods of sudden water velocity increases and facies Ls and Lbr during normal flow conditions on gently sloped ramps and rapids, principally by aggradation. This FA was recognised in the western portion of the outcrop Ocio-1 (Figs. 4B, C; 5F; 11) and in the middle part of Ocio-2-1 (Fig. 5A).

FA 4 mainly formed in dammed areas along the channel and floodplain inhabited by hydrophilous rooted vegetation, here referred to palustrine conditions (*cf.* Ajuaba *et al.*, 2021; Arenas *et al.* 2014b). Extensive development of hydrophilous up-growing plants produced dense stem phytoherms (Lst 1); the already calcite-coated portions of the plants could be broken during disruption by gentle water currents, and their fragments accumulated in nearby areas as facies Lph, as well as forming oncoidal deposits (Lo). Slow-flowing water areas among the vegetated zones were favourable for fine sediment accumulation and fauna survival (facies Sb). The density of facies Lst 1 accounts for the presence of thriving marshy vegetation and facies Sb reflects sluggish water throughout the area. Flooding of vegetated areas could result from water level increases during rainy seasons and/or by aggradation of downstream barrages, a case described in Holocene deposits of the Añamaza Valley (Arenas *et al.*, 2014b). Thus, this FA indicates palustrine conditions in extensive areas, for example, in the southwestern part of Ocio-1 (Figs. 4A, B; 8D, E, F; 11) and in some intervals of Ocio-2 (Fig. 5A). In some Mediterranean regions (Ajuaba *et al.*, 2021; Arenas *et al.*, 2014b; Henchiri, 2014; Vázquez-Urbez *et al.*, 2012; Violante *et al.*, 1994) and in southern Portugal (Fernandes *et al.*, 2023; Guerreiro, 2015) similar facies associations have been described.

Pleistocene deposits

Several deposits of this age were selected for sedimentological analysis. One was located in the eastern part, where the stratigraphic sections Ocio-1-1 and Ocio-1-2 were measured (Fig. 2). To the North of the road there is *ca* 5.5m thick deposit that consists of laterally related lithosomes, 2 to 2.5m thick and 2.5 to 6m long (Figs. 10; 11). These were formed of either stem phytoherms and phytoclastic tufa (facies Lst 1 and Lph) or banded carbonate sand containing ostracods and gastropods (facies Sb and Lphf), conforming to FA 2 (Figs. 4E; 10). In some of these two types of lithosomes, hemi-domed and lenticular bodies up to 0.5–1m in height, consisting of successive highly inclined moss layers (facies Lbr) are present (FA 1a). In some cases, a lateral passage from the Lbr layers to Sb was observed. The western part of this deposit is composed of decimetre-thick layers of dominant phytoclast rudstones (Lph and Lphf) and interbedded patches of stem boundstones (Lst 1) that fit FA 2. The same pattern continued laterally over 10–20m to the West of the image, as shown in Figure 10. On the southern side of the road (Fig. 11), about 12m South of the outcrop illustrated in Figure 10, stands a 2.5m thick body mainly consisting of highly inclined layers formed of facies Lbr and Lst 2, with clear progradation over banded facies Sb and Lb (Fig. 4D, G), representing a vertical cascade over a dammed area, that is, FA 1b (Fig. 15).

Therefore, these Pleistocene outcrops represent small, shallow pools (facies Sb and Lphf) between barrages consisting of stem phytoherms (facies Lst 1). Moss mats (forming both cushions and lenticular bodies) that lived primarily on the upstream side of the small pools formed vertical cascades with overhangs in the pooled zones. In this situation, the downgrowing and low-angle stems gave rise to facies Lst 2. The occurrence of a series of small pools between small barrage cascades (FA 1a) and between barrages formed mainly of facies Lst 1 (FA 2) reflects low- to slightly moderate-slope stretches of the river course (Fig. 10) in the eastern portion of the Pleistocene outcrop. However, the total height of the barrage cascades on the upstream side was unknown because of the lack of outcrops.

In this respect, it is worth noting that to the East of the outcrop in Figure 10, larger pools should have existed, that is, between Ocio-1 and the locality of Ocio. At present, most of this zone is represented by a whitish flat area, with poorly exposed loose-tufa outcrops labelled as "Quaternary to recent alluvial and loose tufa" in Figure 2A. Part of this area likely corresponds to deposition in water held back by prograding-aggrading barrage-cascades, similar to those in the easternmost part of Ocio-1 (Fig. 10). In fact, the upper half of section Ocio-1-1, some 12m above the road, contains gastropods and charophyte-stem wackestones (Fig. 13F).

The deposits to the West and on the southern side of the road, where stratigraphic section Ocio-1-4 were measured (Fig. 2 for location; Fig. 5B), consist of up to 3m thick of centimetre- to decimetre-thick beds formed of laterally related palisades or patches of up-growing stems (Lst 1), and phytoclast accumulations (Lph and Lphf) (Fig. 11), which fit FA 4. A 4m wide and ≈0.6m thick lenticular

body consisting of banded and laminated carbonated sands and fine phytoclasts (Sb and Lphf) is limited laterally by irregular accumulations of phytoclasts (Lph) and oncoids (Lo), and by beds consisting of dominant facies Lst 1. Finely laminated tufa (Ls) occurs on the eastern side of the lenticular body and the laminae are gently inclined to the Southwest (FA 3) (Fig. 11).

The western part of the Pleistocene outcrop represents dominantly palustrine conditions, with water pooled between barrages consisting of facies Lst 1 and Lph (Fig. 4A; FA 3). The lenticular body formed in a shallow pool with slow-flowing water where banded facies Sb and Lphf developed. At the upstream margin of the pool, microbial mats produced conspicuous laminations inclined toward the pool and parallel to the water flow (West and Southwest). In the lateral relation to the above-described deposit, tabular and lenticular beds consisting of stromatolites and fine phytoclasts up to 1m thick were found (Fig. 4C, F), mainly fitting FA 3.

Holocene deposits

Holocene deposits are less favourable for detailed sedimentological drawings than Pleistocene deposits because of the lack of good and continuous outcrops. The deposits in Ocio-2 are principally formed of, i) facies Sb associated with Lbr and up to 1m thick Ls deposits, conforming to FA 1a and ii) facies Lst 1 and Lph, with minor Lo, fitting FA 4. The deposits of FA 1a and FA 4 occurred alternately over time, suggesting episodes of change in the water flow conditions. In the Herrerías Zone, the outcropping Holocene deposits correspond to stepped cascades and dammed areas, as shown in FA 1c (Fig. 6).

Proposal of a sedimentary facies model

The scarcity of well-preserved tufa outcrops along the Inglares Valley has limited studies to the El Tobal and Herrerrías zones in the lower and upper stretches of the valley, respectively (Figs. 2; 3). At present, the riverbed slope is much less steep in the lower stretch than in the upper stretch of the valley (1.01% for segments C and D vs. 4.24% for segment B; Fig. 3). These present slope features are highly consistent with the depositional conditions indicated by the dominant facies found in the studied tufa at each stretch, suggesting that the depositional conditions during the previous Quaternary tufa-forming periods could mimic the present riverbed configuration. This has also been observed in other tufa records from the Mediterranean region (*e.g.* Arenas *et al.*, 2014b; Pedley, 2009).

Together, the aforementioned features indicate that the studied Quaternary tufa deposits along the Inglares Valley were formed in two distinct depositional situations. A single model integrating these two distinct situations was developed based on the main sedimentological features found in different outcrops, independent of age (Fig. 16).

1) The low- to moderate-slope depositional setting, with standing water areas dammed by barrage cascades and palustrine zones, is represented by the El Tobal zone. In Ocio-1 and Ocio-2, the tufa deposits are interpreted to have formed in the distal or lower portion of a fluvial valley over a gently stepped riverbed consisting of a main channel with short cascade structures, eventually with localised barrage-cascades and slow-flowing and standing water zones. The context fits a low to slightly moderate sloped stretch with shallow channels and narrow floodplains in which flourishing palustrine conditions exist and pools develop. The sedimentological features of Ocio-1 and Ocio-2 are very similar; thus, they are considered together in Figure 16. The most significant features of this depositional setting are as follows:

i) The absence of coarse detrital deposits at the base of the tufa deposits might indicate the low competence of water courses at the distal position within the depositional area with respect to the upstream source. Nonetheless, the contact between the oldest tufa and bedrock does not outcrop.

ii) Formation of short barrages from phytoherms and pools along the riverbed. Short barrage-cascades and cascades consisting of moss boundstones and minor stromatolites represent small jumps or knickpoints along the river course with slowly flowing water pooled backward.

iii) Ocurrence of dammed water areas in which carbonate sand and silt accumulate and fauna and flora throve.

iv) Common palustrine conditions associated with sluggish water in shallow pools along the channel and floodplain.

v) Low-slope channel areas with free-flowing water that experience changes in flow conditions. Enhanced disruption of plant boundstones during high water energy and microbial and moss mat development under normal or regular water flow. These changing conditions were recorded in alternating phytoclastic and microbialitic laminated deposits.

Other Quaternary fluvial tufa systems in the Mediterranean region (Buccino *et al.*, 1978; Capezzuoli *et al.*, 2014; Henrichi, 2014; Pedley *et al.*, 2003; Violante *et al.*, 1994) have been reported to fit either fully or partially within the low- to moderate-slope depositional context described above. In northeastern Spain, the Holocene tufas in the Piedra and Añamaza Rivers (Arenas *et al.*, 2014b;

Vázquez-Urbez *et al.*, 2012) and the Pleistocene tufas of the distal portion of the Ebrón River (Ajuaba *et al.*, 2021) and Mesa River (Vázquez-Urbez *et al.*, 2012) present many similar features, but also some differences with respect to the present case. Regarding tufa deposition in the distal portions of the valleys, the most conspicuous differences were: 1) the lack of facies containing organic matter (peat), that is, the absence or no preservation of deposits from stagnant conditions in the Inglares Valley. This suggests very shallow conditions with frequent water renewal and/or continuous flow and 2) the presence of short cascades and barrage-cascades in the Inglares Valley. Together, these features indicate a slightly higher slope in some parts of the distal Inglares valley, compared with the aforementioned cases, as being responsible for the different depositional conditions or subenvironments.

2) The high-slope depositional setting, consisting of steep stepped cascades, barrage cascades, and dammed areas, is represented in the Herrerías Zone. The Quaternary deposits along segment B (Fig. 3) of the Inglares Valley formed on a steep riverbed zone consisting of stepped cascades, corresponding to mostly aggrading structures forming barrage-cascades and slow-flowing and standing water zones upstream. The most conspicuous features of the stepped cascades are as follows:

i) Presence of coarse detrital deposits (facies G), representing increasing flow conditions and erosion, interbedded with tufa facies.

ii) Absence of stem bioherms (that is Lst 1 and Lst 2) and abundance of large phytoclasts coated and uncoated by laminated calcite (Lph). These features suggest the breaking and falling of stems and trunks in relation to high discharge and/or steep slopes, being deposited almost on-site or after short transport.

iii) Abundant stromatolites forming irregular, highly inclined bodies, denoting fast-flowing water on steep surfaces.

In the dammed water areas upstream and downstream of the cascades, where fauna and flora throve, carbonate sand and silt accumulated along with some carbonaceous debris. Larger and thicker Sb deposits were preserved at the top of the steep-stepped structure, indicating the development of downstream barrage-cascades.

These characteristics have also been recognised in other Quaternary tufa systems in the Iberian Ranges, such as the Pleistocene high-slope tufa model in the Añamaza Valley (Arenas *et al.*, 2014b) and Holocene tufas in the Las Parras River Valley (Rico *et al.*, 2013). In both examples, the largest tufa build-ups developed along the waterfalls which formed in relation to changes in bedrock lithology and structure. Tufa deposits associated with high slope settings mirror those described by Violante *et al.* (1994) in the Quaternary fluvial systems of southern Italy.

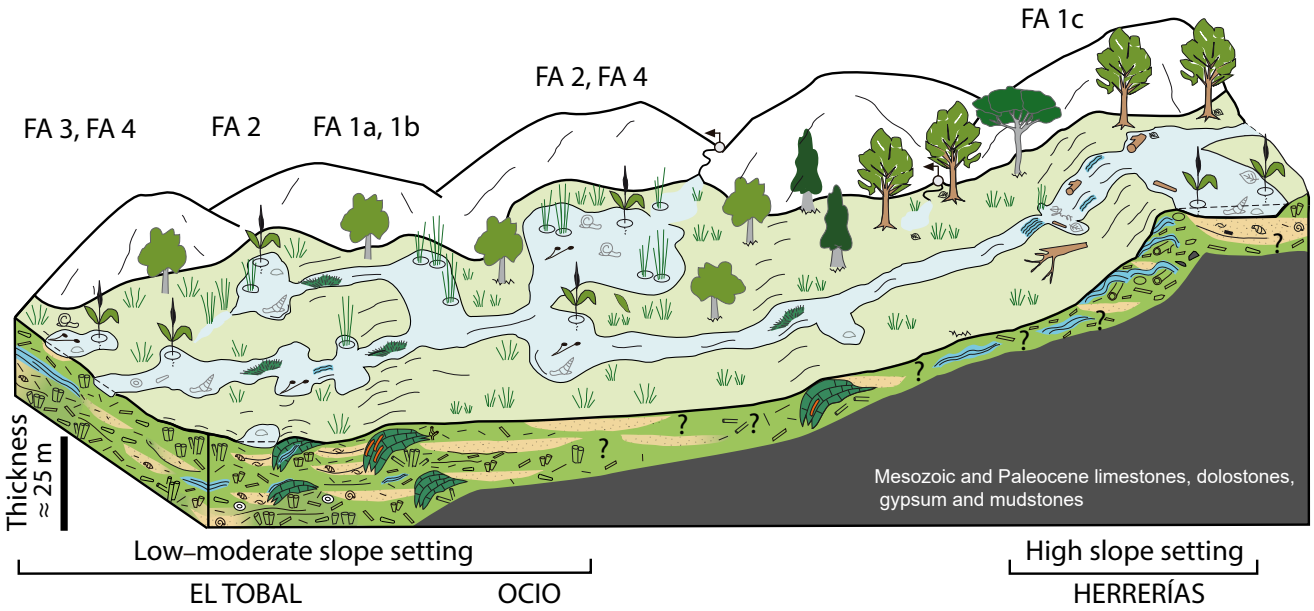

FIGURE 16. Sedimentary facies model for the studied tufas along the Inglares River valley. Two main depositional settings are expressed: low to moderate and high slope settings. Question marks indicate tentative depositional interpretation for the areas without tufa outcrops. FA: Facies Associations. Legend for symbols in Figure 15.

Factors that controlled the Inglares River tufa formation

Among the factors that influence the formation of fluvial tufas are climate, tectonics, and bedrock composition and structure; some aquifer characteristics rely on extrinsic factors (Arenas-Abad *et al.*, 2010; Arenas *et al.*, 2014b; Capezzuoli *et al.*, 2014; Della Porta, 2015; Töker, 2017; Viles *et al.*, 2007). Depending on the extrinsic factors and acting on different scales, the intrinsic factors include the development of hydrophilous flora, physical and chemical properties of water, and CO_2 degassing (Arenas-Abad *et al.*, 2010; Auqué *et al.*, 2013; Melón and Alonso-Zarza, 2018; Pentecost, 2005). Some parameters affect tufa formation at different timescales, imprinting both cyclic and non-cyclic climate signatures on the deposits, such as temperature (Arenas and Jones, 2017).

Climate has been shown to control tufa formation at different scales (Andrews *et al.*, 1997; Arenas-Abad *et al.*, 2010). In the long term, climate controlled the periods with most tufa development during the Quaternary. Many tufa deposits coincide with warm periods, represented by odd marine isotope stages (Garnett *et al.*, 2004; Martín-Algarra *et al.*, 2003; Tagliasacchi and Kaysery-Özer, 2020). In this sense, the studied tufa deposits in the Inglares River correspond to MIS 5e, an overall warm period with abundant preserved tufa deposits worldwide, and MIS 1, also featured as a warm and humid period with decreasing humidity conditions over time (cf. Andrews *et al.*, 2000). The stable isotope composition of the studied deposits herein allows some climatic and hydrological inferences for the Middle–Late Pleistocene and Holocene, which agrees with other studies. This will be discussed below (section of C and O stable isotope composition).

As it has been shown by studies of recent tufa-forming streams, water composition for calcite to precipitate has to be saturated in Ca^{+2} and HCO_3^- (Auqué *et al.*, 2013, 2014; Kano *et al.*, 2007; Kawai *et al.*, 2006). In the case of the Quaternary Inglares River, this requirement was assured by the occurrence of extensive limestone units of the Cretaceous to Palaeocene age and the karstic nature of the sourced Sierra de Cantabria aquifer. The present-day water composition of the Inglares River is saturated with respect to calcite (see values in Section 2), and tufa deposition occurs along some stretches, for example, within the *Water route* and where the present river flows through the Ocio-2 deposits.

These and other studies have demonstrated that calcite saturation levels increase with higher river slopes, that is, in areas where water velocity and turbulence enhance CO_2 loss, thus promoting the physicochemical precipitation of calcite (Auqué *et al.*, 2014; Chen *et al.*, 2004; Drysdale *et al.*, 2002). Moreover, some distance from the springs is usually required for water pCO_2 loss to equilibrate with atmospheric pCO_2, which also favours an increase in pH and calcite precipitation (Chen *et al.*, 2004; Liu *et al.*, 1995; Violante *et al.*, 1994). A statistically significant number of springs showed a negative correlation between spring discharge, calcite saturation, and pH in a limestone region of northern England, Great Britain (Pentecost, 1992). Accordingly, variations in water discharge over time can also influence the distance between catchment springs and the first tufa deposits (Drysdale *et al.*, 2002). In the case of the Inglares River, despite the limited tufa outcrops and lack of precise datings, the tufa location along the valley would fit a higher discharge in the Pleistocene than in the Holocene based on the lack of Pleistocene tufa outcrops in the upstream zone. A similar situation was described in the Añamaza Valley, NE of the Iberian Peninsula (Arenas *et al.*, 2014b).

Bedrock lithology and structure control the characteristics of the aquifer, and thus the river water composition, as well as the slope and width of the river valley, which can affect the depositional architecture of tufa systems (Arenas *et al.*, 2014b; Glover and Robertson, 2003; Rico-Herrero *et al.*, 2013). In southwestern Tunisia, the bedrock configuration and flat topography of the area where the springs emerged favoured the dominant palustrine conditions of some Holocene tufas (Henchiri, 2014).

Regarding the slope and width of the present Inglares Valley, the least steep and widest areas (Figs. 2A; 3) occur in relation to less resistant bedrock, represented by the Upper Triassic gypsum, mudstone, and sandstone beds, and Oligocene alluvial beds. In contrast, reaches with steeper slopes and narrow sections occur in relation to folded, more resistant bedrock composed of Lower Jurassic, Cretaceous, and/or Palaeocene carbonate rocks (Fig. 2A). These two settings correspond approximately to the areas occupied by: i) the Ocio-1 and Ocio-2 outcrops, and the flat zones with Quaternary-recent alluvial deposits and loose tufa (segments A, C and D; Fig. 3) and ii) the Holocene tufa in the upstream portion of the *Water route*, that is, the Herrerías outcrops (segment B; Fig. 3). It is worth noting that the Ocio-1 and Ocio-2 deposits occurred downstream of a short narrow zone or gorge, from which the slope increased slightly (that is, El Tobal in Fig. 3). In general, knickpoints along the riverbed conditioned by the bedrock lithology and structure promote an increase in water velocity, thus water pCO_2 loss, and favour calcite precipitation (Pentecost, 2005; Rico-Herrero *et al.*, 2013). These bedrock knickpoints can be exaggerated by the later growth of tufa-forming cascades (cf. Vázquez-Urbez *et al.*, 2012).

The depositional characteristics indicated by the sedimentary facies and facies associations from Ocio-1, Ocio-2, and Herrerías and the overall features of the valley, as expressed by the proposed facies model (Fig. 16), support that the bedrock lithological and structural features were the principal factors controlling the tufa depositional architecture. These characteristics are consistent with the two depositional settings expressed in the facies model: i) a low- to slightly moderate-sloped stretch of the valley, with small barrage-cascades, dominant palustrine, and small pool environments, represented in the downstream zone of the valley and ii) a high-slope stretch of the valley, with steep stepped cascades and pools and the absence of extensive flat palustrine zones, corresponding to the upstream zone of the valley.

Moreover, the palaeoecological and depositional information derived from microfossil associations fit the aforementioned conditions well. The Ocio-1 assemblage indicates a shallow, clean water body (oligo–mesotrophic) from groundwater rich in bicarbonate and calcium and abundant aquatic vegetation. The presence of *Paralimnocythere psammophila* may be associated with the leaching of calcium sulphate from the Keuper Facies, which crops upstream of the town of Ocio. The three species of gastropods present in Ocio-1 were observed *in visu* samples of Herrerías (Larena *et al.*, 2025), which suggests a similar water composition. Regarding the Ocio-2 assemblage, it appears that the water body conditions required for the taxa described in Ocio-1 are not present in Ocio-2. It is tentatively proposed that the water mass attributes would not be stable; for example, owing to changes in water depth or velocity, optimal conditions would not develop or would be very limited in that area.

Significance of the C and O stable isotope composition

The $\delta^{13}C$ and $\delta^{18}O$ compositions of the studied Inglares tufas are typical of meteoric water, with biogenic CO_2 from vegetation and soils and no significant effects of evaporation (Andrews *et al.*, 1997; Arenas *et al.*, 2014a; Deocampo, 2010). The correlation between $\delta^{13}C$ and $\delta^{18}O$ values is almost absent, which is consistent with continuous water renewal, which avoids the isotopic effects of evaporation on water $\delta^{18}O$, as occurs in hydrologically open systems such as fluvial environments (Deocampo, 2010; Leng and Marshall, 2004; Talbot, 1990).

The $\delta^{18}O$ values showed wide dispersion among the three groups, with similar averages in Ocio-1 and Ocio-2 and lower averages in Herrerías (Fig. 14A, B; Table 3). The dispersion might respond to local depositional conditions, for example, depending on turbulent versus still conditions. The lower values of stromatolites with respect to the rest of the facies may be in accordance with the deposition in zones of continuous flow, such as the cascades and ramps in which facies Ls formed. The lowest $\delta^{18}O$ values of stromatolites were found in Herrerías, which may also be due to their proximity to upstream springs (that is, with ^{16}O-enriched water). In contrast, some Sb facies with slightly higher $\delta^{18}O$ values than other facies might reflect slow water renewal and the mild effects of evaporation in the pools. Indurated bioclastic limestones containing intraclasts (N= 1) have high $\delta^{18}O$ values, which is consistent with evaporation or local dry-out periods. Except for these differences, there was no distinct pattern of $\delta^{18}O$ variation with respect to facies type. The $\delta^{18}O$ dispersion may also represent water temperature oscillations of unknown durations (Osácar *et al.*, 2013).

For each of the three groups, $\delta^{13}C$ dispersion can indicate changes in the CO_2 contribution to Dissolved Inorganic Carbon (DIC) depending on sedimentary conditions, such as local changes due to vegetation development (*e.g.* abundance of vegetation or proximity to palustrine zones), flow conditions (*e.g.* CO_2 loss in turbulent areas), and photosynthesis effects through preferential $^{12}CO_2$ uptake by aquatic biota (Deocampo, 2010; Leng and Marshall, 2004). For instance, in Ocio-1, the lowest $\delta^{13}C$ values were those of facies Lst 1, which is consistent with the large contribution of biogenic-CO_2 in the vegetated zones. Nonetheless, as in the case of $\delta^{18}O$, there was no distinct pattern of $\delta^{13}C$ variation with respect to facies type.

Regarding the average $\delta^{18}O$ values of the three groups, the low values in the Herrerías area might reflect that this area was closer to the water springs than the Ocio-1 and Ocio-2 areas, thus keeping the water $\delta^{18}O$ enriched in ^{16}O relative to the downstream areas. As for the different average $\delta^{13}C$ values of the three groups (Fig. 14A), several causes are possible. High values of tufa $\delta^{13}C$ can be related to aridity, producing slow development and relatively scarce vegetation, greater soil evaporation (decreased soil respiration rate, allowing the entry of isotopically lighter CO_2 deeper into the soil), and increasing the proportion of C4 vs. C3 plants (Andrews *et al.*, 2000; Candy *et al.*, 2012; Garnett *et al.*, 2004). The $\delta^{13}C_{DIC}$ is higher (up to ≈3‰) if groundwater flows in areas dominated by C4 plants (Leng and Marshall, 2004). The water permanence time in the aquifer can also affect calcite $\delta^{13}C$ values; long periods of low recharge may result in higher $\delta^{13}C_{DIC}$ values (Garnett *et al.*, 2004). Among these causes, less humid conditions during the Ocio-2 deposition than in during the Ocio-1 and Herrerías deposition might have caused noticeable tufa $\delta^{13}C$ variations. However, the similar $\delta^{13}C$ average values of Ocio-1 (Pleistocene) and Herrerías (Holocene) (Fig. 14) might respond to other causes.

When comparing the two Holocene groups, their different locations along the valley may explain, at least in

TABLE 3. Average $\delta^{13}C$ and $\delta^{13}O$ values of the carbonate facies analysed in the three studied tufa groups

Sedimentary facies	Number of samples Ocio1+Ocio2 +Herrerías	Ocio-1		Ocio-2		Herrerías	
		$\delta^{13}C$ (‰VPDB)	$\delta^{18}O$ (‰VPDB)	$\delta^{13}C$ (‰VPDB)	$\delta^{18}O$ (‰VPDB)	$\delta^{13}C$ (‰VPDB)	$\delta^{18}O$ (‰VPDB)
Sb	2+3+4	-8.22	-7.54	-7.70	-7.12	-8.29	-7.64
Lb	2+0+0	-8.34	-6.83				
Lbr	1+2+0	-8.38	-7.20	-8.04	-7.36		
Ls	2+2+2	-8.18	-7.40	-7.59	-7.83	-8.97	-8.57
Lo	0+2+0			-8.03	-7.40		
Lph+Lphf	4+2+0	-8.36	-7.31	-7.44	-6.90		
Lst 1	5+1+0	-8.55	-7.27	-7.30	-7.03		
Total N	34						
Average ± St. deviation		-8.37±0.19	-7.26±0.32	-7.71±0.31	-7.28±0.35	-8.51±0.69	-7.95±0.57

part, their isotopic differences (Fig. 14). Herrerías and Ocio-2 were located approximately 8km away, separated by an *ca* 120m step of elevation. CO_2 equilibration of water $\delta^{13}C_{DIC}$ with atmospheric CO_2 from upstream to downstream areas would increase calcite $\delta^{13}C$ values from the Herrerías area to the Ocio-2 area (cf. Osácar *et al.*, 2013). Moreover, this spatial evolution would suit a rise in $\delta^{18}O$ downstream due to ^{16}O-outgassing, which is consistent with the *ca* 0.7‰ $\delta^{18}O$ increase in Ocio-2 (Table 3). Whether this spatial $\delta^{13}C$ difference was related to a change in the proportion of C4 versus C3 plants is unknown. A change in the stream water composition due to additional isotopically enriched water from downstream springs was ruled out because the addition of downstream water should have caused an increase in light isotopes (*e.g.* Auqué *et al.*, 2013). $^{12}CO_2$-enriched water from the recent vegetation cover might have altered the Holocene $\delta^{13}C$ signature of the Herrerías tufas. If so, the initial Herrerías tufa $\delta^{13}C$ signature could have been higher, *i.e.* closer to that of Ocio-2, rather supporting the overall ^{12}CO-depleted water during the Holocene.

Other processes, such as cementation and neomorphism, occur very soon after deposition in the tufa environment and generally do not change the isotopic composition of primary calcite (Pentecost, 2005). These features were avoided during the careful sampling of micrite in this study and are expected not to have changed significantly the isotopic composition of tufas (Andrews *et al.*, 1997).

Increasing calcite $\delta^{13}C$ values throughout the Holocene fluvial tufa record of central Spain were interpreted as an indicator of the intensification of aridity, leading to lower soil respiration and therefore higher $\delta^{13}C$ of soil CO_2 (Andrews *et al.*, 2000), which was coupled with the climatic warming and drying interpretation of the $\delta^{18}O$ values. Other studies have suggested that a change in the proportion of C3/C4 vegetation might have caused higher values of tufa $\delta^{13}C$ in the Late Holocene compared to those in the Early Holocene and the last interglacial (Doran *et al.* 2015). Increased C4 grass increased the soil-CO_2 $\delta^{13}C$ signature, which could be transmitted to the groundwater feeding the Inglares River. In addition, C3 plants grown under water-stressed conditions tend to have higher $\delta^{13}C$ values (Ehleringer, 1988).

Based on the aforementioned facts, it is tentatively proposed that an increase in aridity could have occurred from the Middle–Late Pleistocene to the Middle–Late Holocene based on $\delta^{13}C$. This hypothesis is consistent with climate conditions inferred from facies, pollen and geochemical proxies in lacustrine records in northeastern and eastern Iberia (González-Samperiz *et al.*, 2008; Mediato *et al.*, 2020) and from $\delta^{13}C$ and $\delta^{18}O$ of speleothems in northern Iberia (Bernal-Wormull *et al.*, 2023). In this dry Holocene setting, the spatial evolution of both $\delta^{13}C$ and $\delta^{18}O$ in the river water might explain (at least in part) the isotopic differences between the Herrerías and Ocio-2 deposition, based on the rise of both isotopes in the studied tufa downstream.

Nonetheless, these ideas must be interpreted with caution because of the lack of continuous outcrops and the fact that the ages provided by the AAR are approximate. Complementary studies, such as those based on fauna (gastropods and ostracods) and flora (charophytes and pollen) can help unravel this and other issues.

Climate and hydrology during the last interglacial period and the Late Holocene

The hiatus between the Pleistocene and Holocene records relies on an erosional phase in the study area. Whether this phase is single or multiple remains unknown. There was no clear physical separation between the Ocio-1 and Ocio-2 outcrops, which lacked erosional features. Older tufa deposits potentially existing on the southern side (that is Ocio-2, nowadays only outcropping MIS 1 deposits) had to be eroded before the Middle–Late Holocene. Erosion

could be favoured by abrupt changes in water discharge, a feature that might indicate a highly variable intensity of precipitation, as has been found in tufa formed in semi-arid and arid conditions. Viles *et al.* (2007) described alternating periods of tufa deposition and fluvial downcutting in Holocene–recent deposits in Namibia. In the study area, there was no physical evidence of erosion, and detrital deposits were absent in the Ocio outcrops. Domínguez-Villar *et al.* (2012) reported erosive periods in Holocene tufa deposits in central Spain caused by the lowering of the water table, with a consequent downstream shift of the springs, in response to a decrease in precipitation during transitional climate conditions from the relatively wet Early Holocene to the more arid Late Holocene. A speleothem record in northern Iberia also reported a trend towards drier conditions from 6 and 2.5ka, after humid conditions in the Early Holocene (Bernal-Wormull *et al.*, 2023). Likewise, sedimentological, pollen and geochemistry proxies of lacustrine records in the Northeast of the Iberian Peninsula indicated drier conditions during the Late Holocene (González Sampériz *et al.*, 2008; Mediato *et al.*, 2020).

Within the overall warm MIS 5, the most favourable conditions for tufa development appear to have occurred in the Eemian (MIS 5e: 128–116Ky), when summer insolation at high latitudes was higher than today (Gibbard *et al.*, 2007; Sancho *et al.*, 2015, and citations therein). The amount of precipitation was higher during the early stages of both MIS 5 and MIS 1 (Domínguez-Villar *et al.*, 2011). The optimum climatic conditions during MIS 1 in the Iberian Peninsula were found during the Early Holocene, when the climate was wetter than during the Late Holocene (Domínguez-Villar *et al.*, 2009, 2011; González-Sampériz *et al.*, 2006; Morellón *et al.*, 2009; Moreno *et al.*, 2010). Mediato *et al.* (2020) correlated aridity phases occurring in the western Mediterranean marshes during the last 4ka with small drops in solar activity and surface sea temperature during positive North Atlantic Oscillation periods. Together, these facts are consistent with the climatic and hydrological findings from the studied tufas in Inglares River valley.

Preservation of natural sites

The Quaternary tufas of the Inglares River valley have had great importance over time, since the construction of the Ocio village and Ocio's castle or Lanos Castle to the present day; they have had different uses including rock quarry, raids of wineries in the same tufas for the wine industry, and buildings. Moreover, present river water uses include agriculture and urban supply, and for the last few years, landscape, cultural, educational, and tourism resources. The aim of this section is to highlight the great value of tufas over time as natural, economic, and cultural resources, aiming at their preservation. These tufas are located within two great potential tourism routes in the area: the castle route, which goes from the castle of Portilla to the Lanos castle, and the Berganzo water route (*Water route*). The actual Inglares River valley is a great example of the current formation of tufas which attracts many tourists throughout the year and researchers because of its great scientific interest.

Tufa extraction in the Ocio area for building purposes began with the construction of the Lanos castle (XI century); the remains of the tufa blocks can be seen in its large walls, currently in ruins, along with sandstone blocks. To extract these blocks, a small quarry was built; it covers a large area of the studied outcrop. Tufa quarries are currently in a conservation period within the conservation project of the area's heritage site because of their great geological and cultural interest.

Owing to the number of archaeological studies in this area, evidence of occupation has been found on the southern slope of the Lanos and Portilla hills, which correspond to a long period spanning from the Iron Age to the early Medieval period (11th–12th century) (https://castillodeocio.com/el-castillo/; Solaun Bustintza and Azkarate Garai-Olaun, 2016). In the case of the Ocio fortress, the top of the imposed Lanos rock (644m) was chosen for its location, which controlled two important routes. For many years, this impressive fortification acted as a guardian against the border fickleness of the kingdoms of Navarra and Castilla (https://castillodeocio.com/el-castillo/). Near the outcrops located in the quarry, tufas were carved to construct underground wineries that are currently disused.

Finally, it is worth highlighting the aforementioned *Water route* where tufas are currently forming. Because of the colour of the water and the landscape it presents, it is a great tourist attraction throughout the year. This is a loop of *ca* 10km covering 170m of elevation; it begins and ends in the town of Berganzo village and follows the course of the Inglares River. It is considered one of the most beautiful routes in the region because of its landscape, forests of ancient trees, crystalline waterfalls, and rural towns with a long history. This easy and accessible route for all audiences stands out on the one hand for its charming forests and on the other hand for the waterfalls and small pools that the river course presents (https://rutadelaguaberganzo.eu/).

Historical and archaeological information on the area is abundant and is clearly exposed to tourists through explanatory panels along different routes. Geological information regarding the surrounding rocks, including Ocio tufas, is absent. Therefore, the geological information offered in this study is intended to i) promote scientific knowledge about the ancient depositional, climatic, and hydrological conditions of the Inglares River valley; ii)

encourage the knowledge of ancient tufa by means of understanding the formation of the current tufa along the present riverbed and iii) help in the preservation of tufa records. This geological information, together with studies of the surrounding rocks that are being carried out near the castle route, is intended to be made available on explanation panels to visitors who visit different routes. It also intends to increase the interest of the population in geology and raise awareness regarding the preservation of natural environments.

CONCLUSIONS

The stratigraphic, chronological (AAR), sedimentological, and $\delta^{13}C$ and $\delta^{18}O$ analyses, complemented with palaeontology, of the studied Quaternary tufa deposits along the Inglares River valley have led to the following important conclusions:

Tufa build-ups concentrate as isolated bodies in the uppermost and downmost stretches of the study valley area. These correspond to the Herrerías and El Tobal zones (Ocio-1 and Ocio-2), with thicknesses of 45 and 25m, respectively. Other tufa deposits are poorly exposed on the present riverbanks and floodplains.

The AAR ages indicated two main stages of tufa development: Middle–Late Pleistocene (MIS 5e; Ocio-1), and middle and Late Holocene (MIS 1; Ocio-2 and Herrerías).

A variety of sedimentary tufa facies and minor gravels were distinguished. These were arranged into four facies associations: FA 1) barrages, cascades, and dammed areas; FA 2) shallow barrage (without cascades) and dammed areas; FA 3) low-slope channel (without cascades) and FA 4) vegetated zones in the dammed areas and floodplains (palustrine conditions).

There are two clear depositional settings. i) Low- to moderate-slope depositional settings, with standing water areas dammed by barrage cascades and palustrine zones, are represented in the El Tobal zone. Discrete moss bioherms, phytoclasts, and extensive stem phytoherms are relevant features of this setting. ii) High-slope depositional settings, consisting of steep stepped cascades, barrage-cascades, and dammed areas, are represented in the Herrerías zone. Stromatolites and large phytoclasts are notable features. These two distinct contexts coexisted within the sedimentation area. A single-facies model integrating both settings was developed.

The lithological and structural characteristics of the bedrock were the principal factors affecting the tufa depositional architecture through slope changes and the location of some knickpoints along the valley.

The main water springs from the carbonate rock aquifer were located upstream and provided water with sufficient calcium and bicarbonate to reach the calcite saturation levels a short distance downstream.

The spatial distribution of tufa deposits suggests that river discharge was larger during the Pleistocene than during the Holocene.

Based on $\delta^{13}C$ values, aridity was inferred to have increased from the Middle–Late Pleistocene to the Middle–Late Holocene in this part of the Iberian Peninsula. Within this arid Holocene setting, the isotopic differences between the Herrerías and Ocio-2 tufas could be related (at least in part) to the downstream spatial evolution of $\delta^{13}C$ and $\delta^{18}O$ in the water in the study area.

Warm climate and decreasing humidity coupled with fluvial discharge changes appear to have characterised the Middle–Late Pleistocene and Middle–Late Holocene deposition in the Inglares River valley.

ACKNOWLEDGMENTS

This research was supported by a predoctoral research grant from the University of the Basque Country (UPV/EHU) to Z.L. (the first author). This work was a part of the activities of the GeoTransfer Scientific Group (Aragón Government-University of Zaragoza), Project E32_23R, which provided funding. It is also a contribution to the Consolidated Research Group IT-1602-22 of the Basque Government University Research System. The scanning electron microscopy (C. Gallego Benedicto), optical microscopy and rock preparation services of the University of Zaragoza, Spain (Servicios de Apoyo a la Investigación, SAI), and the Stable Isotope Laboratory (CCIT-UB Serveis and J. Perona Moreno) of the University of Barcelona are thanked for their technical support. The authors are grateful to Dr. Gonzalo Pardo Tirapu, whose comments and suggestions helped improve the quality of this manuscript. Dr. Bover Arnal and Dr. Della Porta are thanked for their careful reviews.

REFERENCES

Ajuaba, S., Arenas, C., Capezzuoli, E., 2021. Sedimentology of Pleistocene palustrine tufas and associated deposits of the Ebrón Valley (Iberian Ranges, Spain). Estudios Geológicos, 77(1), e137. DOI: https://doi.org/10.3989/egeol.44131.593

Andrews, J.E., Riding, R., Dennis, P.F., 1997. The stable isotope record of environmental and climatic signals in modern

terrestrial microbial carbonates from Europe. Palaeogeography, Palaeoclimatology, Palaeoecology, 129, 171-189.

Andrews, J.E., Pedley, M., Dennis, P.F., 2000. Palaeoenvironmental records in Holocene Spanish tufas: a stable isotope approach in search of reliable climatic archives. Sedimentology, 47, 961-978.

Arenas, C., Gutiérrez, F., Osácar, C., Sancho, C., 2000. Sedimentology and geochemistry of fluvial-lacustrine tufa deposits controlled by evaporite solution subsidence in the central Ebro Depression, NE Spain. Sedimentology, 47, 883-909.

Arenas, C., Vázquez-Urbez, M., Auqué, L., Sancho, C., Osácar, C., Pardo, G., 2014a. Intrinsic and extrinsic controls of spatial and temporal variations in modern fluvial tufa sedimentation: A thirteen-year record from a semiarid environment. Sedimentology, 61, 90-132.

Arenas, C., Vázquez-Urbez, M., Pardo, G., Sancho, C., 2014b. Sedimentology and depositional architecture of tufas deposited in stepped fluvial systems of changing slope: Lessons from the Quaternary Añamaza valley (Iberian Range, Spain). Sedimentology, 61, 133-171.

Arenas, C., Jones, B., 2017. Temporal and environmental significance of microbial lamination: Insights from Recent fluvial stromatolites in the River Piedra, Spain. Sedimentology, 64, 1597-1629. DOI: 10.1111/sed.12365

Arenas-Abad, C., Vázquez-Urbez, M., Pardo-Tirapu, G., Sancho Marcén, C., 2010. Fluvial and associated carbonate deposits. In: Alonso-Zarza, A.M., Tanner, L.H. (eds.). Carbonates in continental settings. Amsterdam, Elsevier, 133-175. DOI: 10.1016/S0070-4571(09)06103-2

Auqué, L.F., Arenas, C., Osácar, C., Pardo, G., Sancho, C., Vázquez Urbez, M., 2013. Tufa sedimentation in changing hydrological conditions: the River Mesa (Spain). Geologica Acta, 11(1), 85-102. Website: https://raco.cat/index.php/GeologicaActa/article/view/263720

Auqué, L., Arenas, C., Osácar, C., Pardo, G., Sancho, C., Vázquez-Urbez, M., 2014. Current tufa sedimentation in a changing-slope valley: The River Añamaza (Iberian Range, NE Spain). Sedimentary Geology, 303, 26-48.

Azennoud, K., Baali, A., Brahim, Y.A., Ahouach, Y., 2021. Climate controls on tufa deposition over the last 5000 years: A case study from Northwest Africa. Palaeogeography, Palaeoclimatology, Palaeoecology, 586, 110767. DOI: https://doi.org/10.1016/j.palaeo.2021.110767

Bernal-Wormull, J.L., Moreno, A., Bartolomé, M., Arriolabengoa, M., Pérez-Mejías, C., Iriarte, E., Osácar, C., Spötl, C., Stoll, H., Cacho, I., Edwards, R.L., Cheng, H., 2023. New insights into the climate of northern Iberia during the Younger Dryas and Holocene: The Mendukilo multi-speleothem record. Quaternary Science Reviews, 305, 108006.

Brasier, A.T., Andrews, J.E., Marca-Bell, A.D., Dennis, P.F., 2010. Depositional continuity of seasonally laminated tufas: Implications for $\delta^{18}O$ based palaeotemperatures. Global and Planetary Change, 71, 160-167.

Bright, J., Kaufman, D.S., 2011. Amino acid racemization in lacustrine ostracodes, part I: Effect of oxidizing pre-treatments on amino acid composition. Quaternary Geochronology, 6(2), 154-173. DOI: https://doi.org/10.1016/j.quageo.2010.11.006

Buccino, G., D'Argenio, B., Ferreri, V., Brancaccio, L., Panichi, C., Stanzione, D., 1978. Il travertini della bassa Valle del Tanagrio (Campania): Studio geomorphologico, sedimentologico e geochimico. Bolletino della Societá Geologica Italiana, 97, 617-646.

Candy, I., Adamson, K.R., Gallant, C.E., Whitfield, E., Pope, R., 2012. Oxygen and carbon isotopic composition of Quaternary meteoric carbonates from western and southern Europe: Their role in palaoenvironmental reconstruction. Palaeogeography, Palaeoclimatology, Palaeoecology, 326-328(11), 1-11. DOI: 10.1016/j.palaeo.2011.12.017

Capezzuoli, E., Gandin, A., Pedley, H.M., 2009. Travertines and calcareous tufa in Tuscany (Central Italy). 27th IAS Meeting of Sedimentology, Fieldtrip Guidebook, 129-158.

Capezzuoli, E., Gandin, A., Pedley, M., 2014. Decoding tufa and travertine (fresh water carbonates) in the sedimentary record: The state of the art. Sedimentology, 61, 1-21.

Chen, J., Zhang, D.D., Shijie, W., Tangfu, X., Ronggui, H., 2004. Factors controlling tufa deposition innatural waters at waterfall sites. Sedimentary Geolology, 166, 353-366.

Della Porta, G., 2015. Carbonate build-ups in lacustrine, hydrothermal and fluvial settings: Comparing depositional geometry, fabric types and geochemical signature. In: Bosence, D.W.J., Gibbons, K.A., Le Heron, D.P., Morgan, W.A., Pritchard, T., Vining, B.A. (eds.). Microbial carbonates in space and time: Implications for global exploration and production. London, The Geological Society, 418(Special Publications), 17-68.

Deocampo, D.M., 2010. The geochemistry of continental carbonates. In: Alonso-Zarza, A.M., Tanner, L.H. (eds.). Carbonates in continental settings, geochemistry, diagenesis, and applications. Amsterdam, Elsevier, 62, 1-59.

Dillon, R.T., 2000. The Ecology of Freshwater Molluscs. Cambridge University Press, 509pp. DOI: https://doi.org/10.1017/CBO9780511542008

Domínguez-Villar, D., Fairchild, I.J., Baker, A., Wang, X., Edwards, R.L., Cheng, H., 2009. Oxygen isotope precipitation anomaly inthe North Atlantic region during the 8.2 ka event. Geology, 37(12), 1095-1098.

Domínguez-Villar, D., Vázquez-Navarro, J.A., Cheng, H., Lawrence Edwards, R., 2011. Freshwater tufa record from Spain supports evidence for the past interglacial being wetter than the Holocene in the Mediterranean región. Global and Planetary Change, 77, 129-141.

Domínguez-Villar, D., Vázquez-Navarro, J.A., Carrasco, R., 2012. Mid-Holocene erosive episodes in tufa deposits from Trabaque Canyon, central Spain, as a result of abrupt arid climate transitions. Geomorphology, 161-162, 15-25.

Doran, T.L.D., Herries, A.I.R., Hopley, P., Sombroek, H., Hellstrom, J., Hodge, E., Kuhn, B.F., 2015. Assessing the paleoenvironmental potential of Pliocene to Holocene tufa deposits along the Ghaap Plateau escarpment (South Africa) using stable isotopes. Quaternary Research, 84(1), 133-143.

Drysdale, R.N., Taylor, M P., Ihlenfeld, C., 2002. Factors controlling the chemical evolution of travertine-depositing rivers of the Barkly karst, Northern Australia. Hydrological Processes, 16, 2941-2962.

Durán, J.J., 1989. Geocronología de los depósitos asociados al karst en España. In: Durán, J.J., Martínez, J. (eds.). El karst en España. Monografías Sociedad Española de Geomorfología, 4, 243-256.

Ehleringer, J.R., 1988. Carbon isotope ratios and physiological processes in arid land plants. In: Rundel, P.W., Ehleringer, J.R., Nagy, K.A. (eds.). Applications of Stable Isotope Ratios to Ecological Research. New York, Springer-Verlag, 41-54.

Fernandes, J.P., Arenas, C., Ortiz, J.E. 2023. Quaternary fluvial carbonate deposits of the Almonda River Valley, Central Portugal. Journal of Iberian Geology, 49, 133-167.

Garnett, E.R., Andrews, J.E., Preece, R.C., Dennis, P.F., 2004. Climatic change recorded by stable isotopes and trace elements in a British Holocene tufa. Journal of Quaternary Science, 19(3), 251-262. DOI: https://doi.org/10.1002/jqs.842

Glover, C., Robertson, A.H.F., 2003. Origin of tufa (cool-water carbonate) and related terraces in the Antalya area, SW Turkey. Geological Journal, 38(3-4), 329-358.

González-Sampériz, P., Valero-Garcés, B.L., Moreno Caballud, A., Jalut, G., García-Ruiz, J.M., Martí Bono, C.E., Delgado Huertas, A., Otto, T., Dedoubat, J.J., 2006. Climate variability in the Spanish Pyrenees during the last 30,000 yr revealed by the El Portalet sequence. Quaternary research, 66(1), 38-52.

González-Sampériz, P., Valero-Garcés, B.L., Moreno, A., Morellón, M., Navas, A., Machín, J., Delgado-Huertas, A., 2008. Vegetation changes and hydrological fluctuations in the Central Ebro Basin (NE Spain) since the late Glacial period: Saline lake records. Palaeogeography, Palaeoclimatology, Palaeoecology, 259, 157-181.

Gradziński, M., 2010. Factors controlling growth of modern tufa: Results of a field experiment. In: Pedley, H.M., Rogerson, M. (eds.). Tufas and Speleothems: Unravelling the microbial and physical controls. London, The Geological Society, 336 (Special Publications), 143-191. DOI: 10.1144/SP336.8

Guerreiro, P.M.O., 2015. Tufos calcários no Algarve central: geomorfologia, sedimentologia e paleoambientes. Ph.D. Thesis. Coimbra (Portugal), University of Coimbra, 361pp. Website: http://hdl.handle.net/10316/26296

Hearty, P.J., O'Leary, M.J., Kaufman, D.S., Page, M.C., Bright, J., 2004. Amino acid geochronology of individual foraminifer (Pulleniatina obliquiloculata) tests, north Queenland margin, Australia: a new approach to correlating and dating Quaternary tropical marine sediment cores. Paleoceanography, 19, 4022. DOI: https://doi.org/10.1029/2004PA001059

Heimann, A., Sass, E., 1989. Travertines in the northern Hula Valley, Israel. Sedimentology, 36, 95-108. DOI: 10.1111/J.1365-3091.1989.TB00822.X

Henchiri, M., 2014. Quaternary paludal tufas from the Ben Younes spring system, Gafsa, southwestern Tunisia: interactions between tectonics and climate. Quaternary International, 338, 71-87. DOI: https://doi.org/10.1016/j.quaint.2013.12.024

Kano, A., Hagiwara, R., Kawai, T., Hori, M., Matsuoka, J., 2007. Climatic conditions and hydrological change recorded in a high-resolution stable-isotope profile of a recent laminated tufa on a subtropical island, southern Japan. Journal of Sedimentary Research, 77, 59-67.

Kaufman, D.S., 2000. Amino acid racemization in ostracodes. In: Goodfriend, G.A., Collins, M.J., Fogel, M.L., Macko, S.A., Wehmiller, J.F. (eds.). Perspectives in amino acids and protein geochemistry. Oxford, University Press, 145-160.

Kaufman, D.S., 2003. Amino acid paleothermometry of Quaternary ostracodes from the Bonneville Basin, Utah. Quaternary Science Reviews, 22, 899-914.

Kaufman, D.S., 2006. Temperature sensitivity of aspartic and glutamic acid racemization in the foraminifera Pulleniatina. Quaternary Geochronology, 1, 188-207.

Kaufman, D.S., Manley, W.F., 1998. A new procedure for deter mining DL amino acid ratios in fossils using reverse phase liquid chromatography. Quaternary Geochronology, 17, 987-1000.

Kawai, T., Kano, A., Matsuoka, J., Ihara, T., 2006. Seasonal variation in water chemistry and depositional processes in a tufa-bearing stream in SW-Japan, based on 5 years of monthly observations. Chemical Geology, 232(1), 33-53.

Kosnik, M.A., Kaufman, D.S., 2008. Identifying outliers and assessing the accuracy of amino acid racemization measurements for geochronology: II. Data Screening. Quaternary Geochronology, 3, 328-341.

Laabs, B.J.C., Kaufman, D., 2003. Quaternary highstands in Bear Lake Valley, Utah and Idaho. Geological Society of America Bulletin, 115(4), 463-478. DOI: 10.1130/0016-7606(2003)115<0463:QHIBLV>2.0.CO;2

Larena, Z., Sanjuan, J., Pascual, A., Rodríguez-Lazaro, J., Larraz, M., Arenas, C., Baceta, J.I., Murelaga, X., 2025. Estudio paleontológico de las tobas cuaternarias de Ocio (Álava, Cuenca Miranda-Trebiño). Geogaceta, 77, 83-86.

Leng, M.J., J.D. Marshall., 2004. Palaeoclimate interpretation of sTable isotope data from lake sediment archives. Quaternary Science Reviews, 23(7), 811-831.

Liu, Z., Svensson, U., Dreybrodt, W., Daoxian, Y., Buhmann, D., 1995. Hydrodynamic control of inorganic calcite precipitation in Huanglong Ravine, China: Field measurement and theoretical prediction of deposition rates. Geochimica Et Cosmoschimica Acta, 59, 3087-3097.

Martín-Algarra, A., Martín-Martín, M., Andreo, B., Julià, R., González-Gómez, C., 2003. Sedimentary patterns in perched spring travertines near Granada (Spain) as indicators of the paleohydrological and paleoclimatological evolution of a karst massif. Sedimentary Geology, 161, 217-228. DOI: https://doi.org/10.1016/S0037-0738(03)00115-5

Matsuoka, J., Kano, A., Oba, T., Watanabe, T., Sakai, S., Seto., K., 2001. Seasonal variation of stable isotopic compositions recorded in a laminated tufa, SW Japan. Earth and Planetary Science Letters, 192, 31-44.

McCrea, J.M., 1950. On the isotope chemistry of carbonates and a paleotemperature scale. Journal of Chemical Physics, 18, 849-857.

Mediato, J.F., Santisteban, J.I., del Moral, B., Mediavilla, R., Dabrio, C.J., 2020. Aridity events during the last 4000 years in Western Mediterranean marshes (Almenara and Benicasim marshes, E Spain). Quaternary International, 566-576, 303-314.

Melón, P., Alonso-Zarza, A.M., 2018. The Villaviciosa tufa: a scale model for an active cool water tufa system, Guadalajara (Spain). Facies, 64(1), 1-16.

Morellón, M., Valero-Garcés, B., Vegas-Villarrúbia, T., González-Sampériz, P., Romero, O., Delgado-Huertas, A., Mata, P., Moreno, A., Rico, M., Corella, J.P., 2009. late glacial and Holocene palaeohydrology in the western Mediterranean region: The Lake Estanya record (NE Spain). Quaternary Science Reviews, 28, 2582-2599.

Moreno, A., Stoll, H., Jiménez-Sánchez, M., Cacho, I., Valero-Garcés, V., Ito, E., Edwards, R.L., 2010. A speleothem record of glacial (25–11.6 kyr BP) rapid climatic changes from northern Iberian Peninsula. Global and Planetary Change, 71, 218-231.

Ordóñez, S., Cuevas, J., Benavente, D., García-del-Cura, M.A., 2016. Architecture of Pleistocene fluvial tufa systems associated with waterfalls: El Salt (Alcoy, Spain). Geogaceta, 59, 7-10.

Ordóñez, S., García-del-Cura, M.A., 1983. Recent and Tertiary fluvial carbonates in Central Spain. Modern and ancient fluvial systems, 485-497.

Ortiz, J.E., Torres, T., Julià, R., Delgado, A., Llamas, F.J., Soler, V., Delgado, J., 2004. Numerical dating algorithms of amino acid racemization ratios from continental ostracodes. Application to Guadix-Baza basin (southern Spain). Quaternary Science Reviews, 23(5-6), 717-730.

Ortiz, J.E., Torres, T., Pérez-González, A., 2013. Amino acid racemization in four species of ostracodes: Taxonomic, environmental, and microstructural controls. Quaternary Geochronology, 16, 129-143.

Ortiz, J.E., Torres, T., Ramallo, S.F., Ros, M., 2015. Algoritmos de datación por racemización de aminoácidos de ostrácodos del Holoceno y Pleistoceno superior en la Península Ibérica. Geogaceta, 58, 59-62.

Osácar, M.C., Arenas, C., Vázquez-Urbez, M., Sancho, C., Auqué, L.F., Pardo, G., 2013. Environmental Factors Controlling the $\delta^{13}C$ and $\delta^{18}O$ Variations of Recent Fluvial Tufas: A 12-Year Record from the Monasterio de Piedra Natural Park (Ne Iberian Peninsula). Journal of Sedimentary Resesearch, 83, 309-322.

Pedley, H.M., 1990. Classification and environmental models of cool freshwater tufas. Sedimentary Geology, 68, 143-154.

Pedley, M., 2009. Tufas and travertines of the Mediterranean region: A testing ground for freshwater carbonate concepts and developments. Sedimentology, 56, 221-246.

Pedley, H.M., González-Martín, J.A., Ordóñez, S., García del Cura, M.A., 2003. Sedimentology of Quaternary perched springline and paludal tufas: Criteria for recognition, with examples from Guadalajara Province, Spain. Sedimentology, 50, 23-44.

Pentecost, A., 1992. Carbonate chemistry of surface waters in a temperate karst region: the southern Yorkshire Dales, UK. Journal of Hydrology, 139, 211-232.

Pentecost, A., 2005. Travertine. Berlin, Springer-Verlag, 445pp.

Portero, J.M., Ramírez del Pozo, J., Aguilar, M., 1978. Mapa Geológico de España, sheet n. 169 (Casalarreina), E 1:50,000. Madrid, Instituto Geológico y Minero de España (IGME).

Portero, J.M., Ramírez del Pozo, J., Aguilar, M., 1979. Mapa Geológico de España, sheet n. 170 (Haro), E 1:50,000. Madrid, Instituto Geológico y Minero de España (IGME).

Rico-Herrero, M., Sancho-Marcén, C., Arenas-Abad, M.C., Vázquez-Urbez, M., Valero-Garcés, B.L., 2013. El sistema de barreras tobáceas holocenas de las Parras de Martín (Cordillera Íberica, Teruel). Cuadernos de Investigación Geográfica, 39(1), 141-158.

Rodríguez-Berriguete, A., Alonso-Zarza, A.M., Martín-García, R., Cabrera, M.C., 2018. Sedimentology and geochemistry of a human-induced tufa deposit: Implications for palaeoclimatic research. Sedimentology, 65, 2253-2277.

Rodríguez-Berriguete, A., Camuera, J., Alonso-Zarza, A.M., 2021. Carbonate tufas as archives of climate and sedimentary dynamic in volcanic settings, examples from Gran Canaria (Spain). Sedimentology, 69, 199-218.

Sallam, E.S., 2022. Facies and early diagenesis of rainwater-fed paleospring calcareous tufas in the Kurkur oasis area (southern Egypt). Carbonates and Evaporites, 37, 46. DOI: https://doi.org/10.1007/s13146-022-00792-3

Sancho, C., Arenas, C., Vázquez-Urbez, M., Pardo, G., Lozano, M.V., Peña-Monné, J.L., Hellstrom, J., Ortiz, J.E., Osácar, M.C., Auqué, L., Torres, T., 2015. Climatic implications of the Quaternary fluvial tufa record in the NE Iberian Peninsula over the last 500 ka. Quaternary Research, 84(3), 398-414.

Solaun Bustintza, J.L., Azkarate Garai-Olaun, A., 2016. El castillo de Portilla (Zambrana, Álava). Origen y significado de una fortaleza plenomedieval en territorio alavés (siglos XI-XII). Munibe Antropologia-Arkeologia, 67, 167-183.

Tagliasacchi, E., Kaysery-Özer, M.S., 2020. Multidisciplinary approach for palaeoclimatic signals of the non-marine carbonates: The case of the Sarıkavak tufa deposits (Afyon, SW-Turkey). Quaternary International, 544, 41-56.

Talbot, M.R., 1990. A review of the palaeohydrological interpretation of carbon and oxygen isotopic ratios in primary lacustrine carbonates. Chemical Geology: Isotope Geoscience section, 80, 261-279.

Töker, E., 2017. Quaternary fluvial tufas of Sarıkavak area, southwestern Turkey: Facies and depositional systems. Quaternary International, Non-Marine Carbonates, 437(Special Issue), 37-50.

Torres, T., Llamas, J., Canoira, L., García-Alonso, P., García-Cortés, A., Mansilla, H., 1997. Amino acid chronology of the Lower Pleistocene deposits of Venta Micena (Orce, Granada, Andalusia, Spain). Organic Geochemistry, 26, 85-97.

Vázquez-Urbez, M., Arenas, C., Pardo, G., 2012. A sedimentary facies model for stepped, fluvial tufa systems in the Iberian Range (Spain): The Quaternary Piedra and Mesa valleys. Sedimentology, 59, 502-526.

Vera y López, V., 1915-1921. «Río Inglares». In: Carreras y Candi, F. (ed.). Geografía general del País Vasco-Navarro

III. Barcelona, Establecimiento Editorial de Alberto Martín, 29pp.

Viles, H.A., Taylor, M.P., Nicoll, K., Neumann, S., 2007. Facies evidence of hydroclimatic regime shifts in tufa depositional sequences from the arid Naukluft Mountains, Namibia. Sedimentary Geology, 195, 39-53.

Violante, C., Ferreri, V., D'Argenio, B., Golubic, S., 1994. Quaternary travertines at Rocchetta a Volturno (Isernia, central Italy). Facies analysis and sedimentary model of an organogenic carbonate system. Ischia (Italy), 15th lAS Regional Meeting, Excursion A1, 21pp.

Manuscript received August 2024;
revision accepted March 2025;
published Online May 2025.

APPENDIX

TABLE I. Sedimentary facies: description of main features and depositional interpretation

Facies and abundance (Figures) Colour	Geometry of deposits	Microstructure, textural characteristics and components	Sedimentary structures	Identifiable biological content	Common associated facies	Depositional sedimentary context
Stromatolites. **Ls** ■■ (Figs. 4F; 6C, D, E; 9B, E, F) Beige and whitish	Lenticular and tabular deposits, with flat to undulate base and top. Single bodies 0.05 to 0.4 m thick. Metres to dam in lateral extent.	Laminated microbial boundstones. Undulate and irregular, alternating light (microspar) and dark (micrite) calcite laminae, up to 2 mm thick. Filamentous micrite bodies arranged as palisades and bush- and fan-shaped bodies, subperpendicular to lamination (Fig. 12E, F).	Flat and undulate lamination	Cyanobacteria and other bacteria. Worm and inset molds.	Lst 1, Sb, Lph and Lbr.	Stream stretches with low to high slope floors over which water flows commonly fast (small jumps, ramps and steeped cascades) and pools. Calcite precipitation on microbes forming microbial mats. Trapping micrite particles?
Oncoidal limestones. **Lo** ■ (Fig. 8F) Beige to light grey	Commonly lenticular bodies, up to 0.3 m thick, decimeters to a few metres in lateral extent.	Oncoid rudstones, commonly including calcite coated phytoclasts and intraclasts. Oncoids are cylindrical and less abundant spherical in shape, up to 3 cm in diameter and 10 cm long. Nuclei mostly made of plant fragments. Calcite coatings a few mm to 1.5 cm thick, formed of light (spar and microspar) and dark (micrite) laminae, with abundant filamentous micrite bodies (tubes) (Fig. 12D, G, H).	Structureless.	Nuclei: fragments of coated macrophytes (higher plant stems). Coatings: Microbial, mostly cyanobacterial.	Lph, Lphf and Sb.	Slow- to moderate-flowing, sometimes dammed water in stream areas. Oncoid accumulation together with Lph in small barrages and pools.
Bioclastic limestones. **Lb** ■ (Fig. 9A) Beige and light grey	Lenticular layers, 0.03 to 0.2 m thick, commonly associated with Sb and Lphf beds. Metres in lateral extent.	Wackestones and packstones, less commonly, floatstones and mudstones, consisting of mostly floral remains (including rare charophyte thalli and gyrogonites), peloids, minor intraclasts, gastropods and ostracods (entire and broken shells) (Fig. 13F).	Structureless.	Fragments of coated and calcified macrophytes, gastropods and ostracods.	Sb and Li	Aggradation in slow flowing and standing water areas along the channel (commonly dammed by barrages) and pools in the palustrine floodplain. Accumulation of calcite sediment from breakage of nearby deposits (e.g., facies Lbr) and from in situ precipitation. Locally, drying out of mud sediment deposited in pools forming hard substrates.
Bioclastic sands and silts. **Sb** ■■■ (Figs. 4A, G; 8A, D; 9A) Beige, white and light to dark grey	Tabular and lenticular beds, up to 0.4 m thick, grouped in sets up to 6 m thick. Metres to decametres in lateral extent.	Lime mud (mostly silt) and fine to coarse sand-size carbonate particles (mostly of flora). Poorly to slightly lithified. Sb may include gastropods, ostracods, oncoids, charophytes, mm-long fragments of plant calcite coatings and intraclasts. Rare carbonaceous debris (Fig. 13D, E). Rare cm-thick Sb layers are compact and hard, and interbedded within the loose sediment.	Structureless or with parallel banding.	Planispiral and trocospiral gastropods (entire and broken), ostracods and charophyte gyrogonites. Small fragments of plant calcite coatings.	Lphf, Lb, Li and Lph	

TABLE I. Continued

Facies and abundance (Figures) Colour	Geometry of deposits	Microstructure, textural characteristics and components	Sedimentary structures	Identifiable biological content	Common associated facies	Depositional sedimentary context
Intraclastic and peloidal limestones. **Li** (■) (Fig. 9A) Beige to orange	Commonly, lenticular patches, rarely beds, up to a few cm thick, and metres in lateral extent.	Packstones and rudstones consisting of massive micrite grains, micrometer to mm long, mostly intraclasts and peloids, along phytoclasts (Fig.13G). In some cases, with ooids.	Structureless.	Unidentifiable	Lph, Lb and Sb	The same as above facies Lb, including breakage of semi-consolidated muddy intervals
Phytoclastic tufa. **Lph** ■■■■ (Figs. 4A; 6B, C, D; 8A, B, D; 9F) Very fine stems (mm long): **Lphf** (Figs. 4A, G; 8A, D, E) ■■■ Beige to light brown	Tabular, undulate and lenticular bodies and patches within beds consisting of Lst 1, up to 0.5 m thick. Decimeters to decametres wide.	Macrophyte rudstones: non-organized, calcite coatings (outer casts) and external molds (imprints) of stems and trunks; leaf imprints. Plants are not preserved (decayed). Minor oncoids can be present. Inner imprints (rounded voids) up to 20 cm in diameter. Laminated coatings around stems and trunks are up to 4 cm thick and consist of light (microspar) and dark (micrite) laminae with filamentous microbial bodies, arranged in palisades and adjacent bush-shaped bodies (Fig. 12A).	Structureless; in some cases, horizontal layering. Groups of stems lying horizontally and parallel to palaeoflow direction.	Fragments and entire parts of macrophytes (trunks, stems and twigs). Gastropods.	Lst 1 and Lbr. Lphf associated with Sb.	Breakage of stem phytoherms and uncoated plants. The debris (most of them already coated by calcite) are transported and deposited close to areas, along channels, at places forming barrage deposits. Leaves accumulated in calm areas. Fine phytoclasts (Lphf) accumulate mainly in dammed areas.
Phytoherm tufas consisting of:						
Stems. **Lst**:						
Bunches. **Lst 1** ■■■ (Figs. 4A; 8D, E, F; 9A, B, D, E) Beige to light brown	Lenticular bodies, commonly patches, 0.05 to 0.5 m thick, decimetres to metres in lateral extent; they form part of tabular and lenticular beds consisting of Lph and Lphf, up to 0.5 m thick.	Boundstones. Bunches and palisades of stems up to 0.5 m high. Vertical or subvertical stems of up-growing macrophytes are coated with laminated calcite, containing microbial evidence (Fig. 12B). In some cases, boundstones of stem imprints (molds).		Portions of macrophytes (rushes, reeds and other grasses)	Lph, Lphf and Lbr	Areas with hydrophilous vegetation; calcite precipitation around the submerged part of plants living in slow-flowing water areas, e.g. dammed areas upstream and downstream of barrages, and banks along the stream.
Curtains and low-angle beds. **Lst 2** ■ (Fig. 4G; 8C) Beige to light yellow	Curtains and low-angle beds commonly formed of a few calcite-coated stems, 0.5 m high and decimetres in lateral extent.	Boundstones formed of stems (macrophytes), set low-angle to vertical (90º), laying parallel to the accumulation surface, coated with laminated calcite.		Hanging and low-angle inclined macrophytes (grasses)	Lph and Lbr	Cascades in which hydrophilous hanging plants (groups of down-growing stems laying parallel to flow) are coated with calcite. Progradation of cascades fronts, occasionally forming over-hangings.

TABLE I. Continued

Facies and abundance (Figures) Colour	Geometry of deposits	Microstructure, textural characteristics and components	Sedimentary structures	Identifiable biological content	Common associated facies	Depositional sedimentary context
Roots. **Lro** (■) (Fig. 9G) Beige to white	Curtains (up to 0.8 m high), resulting from close parallel calcite-coated roots. Metres wide.	Boundstones consisting of mostly vertical and parallel roots, each cm to dm in length, with mm-thick calcite coatings. Calcrete formation.		Roots of macrophytes	Lst 1	Overhanging tufa areas (e.g. jumps and banks) along the stream. The roots of hydrophilous vegetation pass across the overhanging tufa and hang down within the water body, then becoming coated with calcite. Root beds have undergone intense calcrete formation and recent agricultural activities.
Bryophytes. **Lbr** ■■■ (Figs. 4G; 9B, C, D) Beige to light grey	Hemi-domed and lenticular bodies (up to 1 m high), grouped into 2 m thick deposits, resulting from stacking of moss layers. Metres wide.	Boundstones consisting of stacked moss layers (each 1.5-4 cm thick), in which caulidia and phyllidia are coated with calcite. Caulidia are set perpendicular to the accumulation surface and form dense layers (Fig. 13A, B, C).	Banding formed from stacked moss layers (Fig. 9C).	Bryophytes (moss mats) and other minor macrophytes.	Lph, Lst 1, Lst 2 and Sb.	Cascades, jumps along the stream and barrage-cascades with growth of moss mats that are coated with calcite.
Gravels. **G** ■ (Fig. 6D) Beige to light grey	Irregular and lenticular bodies (up to 0.5 m high) Metres wide	Clast-supported, heterometric and angular grains. Consisting of mostly limestones from Cretaceous to Paleocene units. Up to 20 cm long. Matrix absent.	Structureless.	None	Lph (large phytoclasts).	Downhill fall from nearby steep surfaces; high discharge episodes.

(■) Occasional ■ Minor ■■ Common ■■■ Very common ■■■■ Ubiquitous